Alma Mater Studiorum – Università di Bologna

DOTTORATO DI RICERCA IN

SCIENZE E TECNOLOGIE AGRARIE, AMBIENTALI E ALIMENTARI

Ciclo XXXV

Settore Concorsuale: 07/C1 - INGEGNERIA AGRARIA, FORESTALE E DEI BIOSISTEMI

Settore Scientifico Disciplinare: AGR/09 - MECCANICA AGRARIA

COMPUTATIONAL TOOL FOR THREE-POINT HITCH GEOMETRY OPTIMIZATION

Presentata da: Dott. Lianet Avello Fernández

Coordinatore Dottorato	**Supervisore**
Prof. Massimiliano Petracci	Prof. Mirko Maraldi

Esame finale anno 2023

DECLARATION

I hereby declare that the following thesis is the result of my Ph.D. research carried out during a period of three years. Contributions from other authors have been appropriately cited and reported in the bibliography. This dissertation is original and has not been submitted to any other institution or university for the achievement of other qualifications/degree.

Lianet Avello Fernández

Bologna, January 2023

PHRASE

"It always seems impossible until it is done."

Nelson Mandela

ACKNOWLEDGMENT

Before concluding this research journey, I would like to express my deepest gratitude to some people without whom this research would not have been possible:

First, I would like to give my special thanks to my supervisor Professor Mirko Maraldi, whose guidance, support, and encouragement has been invaluable throughout these three years of research work.

Furthermore, I would like to express my gratitude to Professor Michele Mattetti for providing me with his support and encouragement. I am also thankful to the coordinator of this Ph.D. research program Professor Massimiliano Petracci for his direction during all the research process and evaluation courses.

Thanks, should also go to my colleagues from the DISTAL department with whom I have shared so many offices time and to my friends, especially my dear friend Ana, for offering me her unconditional help from the first day of my arrival and sharing with me so many grateful moments during these years.

Last but not the least, I would like to thank to my family for supporting me spiritually throughout this process and in my life in general.

ABSTRACT

The weight-transfer effect, consisting of the change in dynamic load distribution between the front and the rear tractor axles, is one of the most impairing phenomena for the performance, comfort, and safety of agricultural operations. Excessive weight transfer from the front to the rear tractor axle can occur during operation or maneuvering of implements connected to the tractor through the three-point hitch (TPH). In this respect, an optimal design of the TPH can ensure better dynamic load distribution and ultimately improve operational performance, comfort, and safety. In this study, a computational tool (*The Optimizer*) for the determination of a TPH geometry which minimizes the weight-transfer effect is developed. The Optimizer is based on a constrained minimization algorithm. The objective function to be minimized is related to the tractor front-to-rear axle load transfer during a simulated reference maneuver performed with a reference implement on a reference soil. Simulations are based on a dynamic model of the tractor-TPH-implement aggregate. For the modeling of the tractor, two alternatives were studied: a quasi-static model and a 3-degrees-of-freedom (DOF) dynamic model. The inertial, elastic, and viscous parameters of the dynamic model were successfully determined through a parameter identification algorithm. The behavior of the front axle load resulting from both models' simulations was compared with a real front axle load measured during an experimental in-field maneuver. The comparative analysis showed that the dynamic model approach was effective in accurately predicting the actual behavior of the tractor in order to replicate the peak-to-peak on the front axle load. The geometry determined by the Optimizer complies with the ISO-730 Standard functional requirements and other design requirements. The interaction between the soil and the implement during the simulated reference maneuver was successfully validated against experimental data. Simulation results show that the adopted reference maneuver is effective in triggering the weight-transfer effect, with the front axle load exhibiting a peak-to-peak value of 27.1 kN during the maneuver. A benchmark test was conducted starting from four geometries of a commercially available TPH. As result, all the configurations were optimized by above a 10%. The Optimizer, after 36 iterations, was able to find an optimized TPH geometry which allows to reduce the weight-transfer effect by 14.9%.

SUMMARY

NOMENCLATURE TABLE

Symbol	Variable	unit (SI)
c_f	front wheels damping coefficient	N s m^{-1}
C_k	TPH constraint no. k	–
c_r	rear wheels damping coefficient	N s m^{-1}
c_s	front axle suspension damping coefficient	N s m^{-1}
C_{sy}	viscous coefficient for the soil-implement vertical force	N s m^{-1}
d	TPH dimensions vector	–
erf	Gauss error function	–
e_p	peak error between the experimental and simulated front axle load	kN
e_v	valley error between the experimental and simulated front axle load	kN
F_{0x}	offset value for the soil-implement horizontal force	N
F_{0y}	offset value for the soil-implement vertical force	N
F_{cp}	force at the two lift arm link points	N
F_{fw}	front wheels force	N
F_{hc}	hydraulic lift cylinders force	N
F_{lad}	force at the two lower hitch points	N
F_{lap}	force at the two lower link points	N
F_{lr}	lift rods force	N
F_{rw}	rear wheels force	N
F_s	front axle suspension force calculated with the 3-degrees-of-freedom dynamic tractor model	N
$F_{s_{static}}$	front axle suspension force calculated with the quasi-static tractor model	N
F_{ua}	upper arm force	N
F_{wx}	soil-implement force, horizontal component	N
F_{wy}	soil-implement force, vertical component	N
g	gravitational acceleration	m s^{-2}
G_i	implement centre of gravity	–
G_t	tractor centre of gravity	–
h_f	vertical distance between tractor centre of gravity and front axle	m
H_{lad}	height of lower hitch points above the ground	m

H_{ma}	height of lower hitch points above the ground	m
h_r	vertical distance between tractor centre of gravity and rear axle	m
H_T	total traction force	N
I_i^{Gz}	implement moment of inertia	kg m^2
I_t^{Gz}	tractor moment of inertia	kg m^2
k_f	front wheels spring constant	N m^{-1}
k_r	rear wheels spring constant	N m^{-1}
k_s	front axle suspension spring constant	N m^{-1}
K_{sm}	proportionality coefficient for the soil-implement moment	N
K_{sx}	proportionality coefficient for the soil-implement horizontal force	N m^{-1}
K_{sy}	proportionality coefficient for the soil-implement vertical force	N m^{-1}
L	distance between power take-off and lower hitch points	m
L_{14}	lower hitch point height as per ISO-730	m
L_{15}	levelling adjustment as per ISO-730	m
L_{18}	movement range as per ISO-730	m
L_{19}	transport height as per ISO-730	m
L_{20}	lower hitch point clearance as per ISO-730	m
l_c	lift arm length	m
l_{chc}	lift arm cranks length	m
L_{CV}	vertical convergence distance	m
l_f	longitudinal distance between tractor centre of gravity and front axle	m
l_{hc}	hydraulic lift cylinders length	m
L_j	lower bound on dimension d_j	various
L_{wj}	lower bound on dimension w_j	various
l_{la}	lower arm length	m
l_{lalr}	distance of the lift rods link on the lower arms	m
l_{lr}	lift rods length	m
l_r	longitudinal distance between tractor centre of gravity and rear axle	m
l_{ua}	upper arm length	m
M_0	offset values for the soil-implement moment	N m
M_a	front axle unsuspended mass	kg
m_h	mast height	m
M_i	implement mass	kg
M_t	tractor chassis mass	kg
M_w	moment of the soil-implement resultant about point P_{lad}	N m
N_C	number of TPH constraints	–
N_D	number of TPH dimensions subject to optimisation	–
N_w	number of parameters dimensions from the dynamic tractor model subject to optimisation	–
P_{cd}	lift arm – lift rod connection points	–
P_{cp}	lift arm link points	–
P_{hcd}	lift arm – hydraulic lift cylinder connection points	–

P_{hcp}	hydraulic lift cylinder link point	–
P_{lad}	lower hitch points	–
P_{lam}	lift rod – lower link connection points	–
P_{lap}	lower link points	–
P_{tf}	link point of front axle suspension on the tractor chassis	–
P_{tr}	link point of rear wheels hubs on the tractor chassis	–
P_{uad}	upper hitch point	–
P_{uap}	upper link point	–
R_i	radial coordinate of the implement centre of gravity	m
r_{rw}	static loaded radius of the rear wheels	m
T	reference manoeuvre characteristic time	s
t	simulation elapsed time	s
t_0	offset time for reference manoeuvre onset	s
U_j	upper bound on dimension d_j	various
U_{wj}	upper bound on dimension w_j	various
w	dimension vector containing the dynamic tractor model parameters to be identified	–
$\mathrm{X_{P_k}}$	longitudinal coordinate of the point P_k	m
X_{PTO}	power take-off length	m
Y_a	front axle unsuspended mass vertical displacement	m
$Y_{\mathrm{P_k}}$	vertical coordinate of the point P_k	m
γ_i	angular coordinate of the implement centre of gravity	rad
Δ_{min}	lower hitch points clearance	m
θ_t	tractor pitch angle	rad
Φ	objective function from the TPH optimization problem	N
Ψ	objective function from the parameter identification problem	kN
φ_c	lift arm angle	rad
φ_{chc}	lift arms crank angle	rad
φ_{hc}	hydraulic lift cylinder angle	rad
φ_i	implement mast angle	rad
φ_{la}	lower arm angle	rad
φ_{lr}	lift rod angle	rad
φ_{ua}	upper arm angle	rad

CHAPTER 1. INTRODUCTION AND LITERATURE REVIEW

1.1 Research Context

In the past few decades, significant technological advances and changes have occurred in the agricultural tractor market. The demand for more compact tractors with high levels of technology has led to great improvements regarding various tractor's operational aspects such as higher energy efficiency, lower pollutant exhaust gas emission, electrification, autonomous guidance with integrating telematics, environment protection, tractive efficiency, comfort, and safety. However, increasing the complexity level of mechanical systems has constrained designers on the adoption of new advanced design tools such as numerical simulation and optimization. These new techniques allowed agricultural tractors manufacturers to increase their global market competitiveness by ensuring modeling accuracy versus complexity and reduction of cost, and time of production needed for testing and experimentation (Baillie, Lobsey, et al., 2018; Baillie, Thomasson, et al., 2018; Kabir et al., 2014; Previati et al., 2011; Sunusi et al., 2020; Thomasson et al., 2018).

Nowadays, these topics have become of utmost importance for the designers of agricultural machinery and for the market as well. One of the most impairing phenomena in terms of comfort, safety, and tractor's performance during agricultural operations is the dynamic load transfer, also known as the weight transfer effect. Macmillan (2003), defines weight transfer as a normal outcome of the action of the forces generated on the tractor chassis by the ground and by the implement and transmitted to the tractor driving axles through the attachment system. In this regard, the type and design of the hitching system play a significant role in the distribution of dynamic loads during the tractor´s field operations, implement maneuvering, and prevention of fatigue damage. Indeed, implement extraction from the soil

during headland turns the primary cause of fatigue damage during field operation since it induces a significant load change in tractor axles (Mattetti et al., 2017).

The three-point hitch (TPH) attachment system is the most widely used in modern agricultural tractors because of its efficiency in lifting and stabilizing the implement as well as increasing load transfer to the tractor's driving wheels (Molari et al., 2014). For that reason, designers of agricultural machinery often analyze the tractor, the TPH, and the implement as a compound system such that optimal and efficient use of loads could be obtained to accomplish different design purposes focused on the improvement of tractors' operational performance (Bauer et al., 2017; Zheng, Cui, et al., 2019; Zheng, Zhong, et al., 2019).

1.2 Outline of the Thesis

This doctoral thesis is the result of 3-years study summarized in a scientific publication paper called: "*A Computational Tool for Three-Point Hitch Geometry Optimisation Based on Weight-Transfer Minimisation*" (Avello Fernández et al., 2022). The thesis manuscript is structured in the following manner:

- CHAPTER 1: INTRODUCTION AND LITERATURE REVIEW

  Basic concepts and methods are presented in this chapter aiming to gain further understanding on the modeling and design optimization of a TPH and the tractor-implement dynamic performance. Furthermore, a detailed literature review is carried out analyzing different approaches developed in the research field.

- CHAPTER 2: MATERIALS AND METHODS

  This chapter shows the mathematical equations and algorithms necessary for the development of the design tool "*The Optimizer"*. The main equations for the TPH-implement kinematic analysis are described. A dynamic model of an agricultural tractor equipped with a front axle suspension and bearing an implement mounted on the rear TPH is developed. To evaluate the influence of the TPH geometry on the weight transfer, a lifting maneuver is defined for a reference implement on a reference soil. The optimization algorithm used by the design tool is also described.

- CHAPTER 3: RESULTS AND DISCUSSIONS

The validation of the soil-implement interaction model is described as well as the identification of the tractor's parameters needed to perform the simulation of the reference maneuver. Optimization results obtained with the computational design tool are set and analyzed.

- CONCLUSIONS

Based on the results obtained during the research and exposed in the Chapter 3, the conclusions of the present thesis are drawn.

1.3 Three-Point Hitch Design

There are different types of hitching systems, however, the most commonly used in modern tractors is the rear-mounted (TPH) linkage mechanism, composed by two lower links and one upper link (Figure 1.1). The connection of the implement is made through three pivotal articulate connections at the end of each link and the lifting and lowering operations are controlled by the tractor hydraulic system.

Figure 1.1. Rear-mounted three-point hitch structure.

The TPH system was first introduced by Ferguson in the late 1930s, its objective was to take advantage of the dynamic load transfer from the implement and tractor front wheels to add load to the driving wheels on two-wheel drive tractors thus allowing the use of lighters tractors and improving its tractive performance (Molari et al., 2014; Morling, 1979). Compared to other hitching mechanisms, this system provides significant advantages, such as easy implement transportation, depth and draft control, and better weight transfer.

Morling (1979) provides a comprehensive analysis on the understanding of the functional design requirements for a TPH. Some of the main features that a well-mounted TPH should meet to accomplish functional design requirements are: depth control of implement; load transfer to drive wheels; lateral sway and center-ability; inter-changeability of implement and tractor; force and draft leveling of the implement; lateral leveling; limiting sway of implement; locking hitch laterally when in transport or using the power take-off (PTO) with implement or semi-mounted implement; quick and easy attachment and detachment of implement; adequate lifting capacity of the hydraulic system; independent vertical float of each lower link hitch point; pitching the implement as it is raised; simple and easy adjustment of the hitch; among others. Some of these functional requirements are governed by established design standards.

1.3.1 Three-Point Hitch Design Standarization ISO-730

The interest by the majority of tractors manufacturer on the adoption of the TPH system, led to the emergence of design dimensions standards, in particular ASAE and ISO (ASAE Standards, 2001; ISO, 2009). The standards define the geometric design dimensions to ensure compatibility between the tractors and the different types of implements in correspondence with tractor power and wheelbase. There are fundamental differences between ASAE S217.11 and ISO-730 concerning the following areas: 1) implement mast height; 2) PTO to lower hitch point distance; 3) power stroke; 4) mast kick-up and 5) two type of Category 4. As result, designers should be aware of the difference and analyze the final market when selecting the design standard to be used (ASAE Standards, 2001). In the present research work the international standard ISO-730:2009+A1:2014 (referring to "*Agricultural wheeled tractors_ Rear-mounted three-point linkage_Categories 1N, 1, 2N, 2, 3N, 3, 4N and 4"*) (ISO, 2009) have been used as a reference frame for the constraints evaluation on the

geometrical and kinematic design parameters of the TPH, since ISO-730 standard guarantees compatibility with most of the equipment and tractors currently prevailing in the European market. In the Figure 1.2 are represented the components and dimensions of the TPH design according to the ISO-730 standard.

1.3.2 Three-Point Hitch Kinematics

As previously mentioned, the geometrical and kinematic parameters of the TPH design are constrained by international standards. However, some variable margins on these parameters are still provided to the designers so that geometrical dimensions can be customized and optimized to be consistent with the tractor's most advanced functionalities demanded by the agricultural market.

In this regard, different approaches have been proposed for the kinematics analysis of the TPH design. According to Morling (1979), the TPH mechanism in the vertical plane can be considered as a four-bar planar system, where the two lower links are considered to be superimposed: the tractor body constitutes one bar, the two superimposed lower links constitutes the second bar, the upper link and the implement mast constitutes the third and fourth bars.

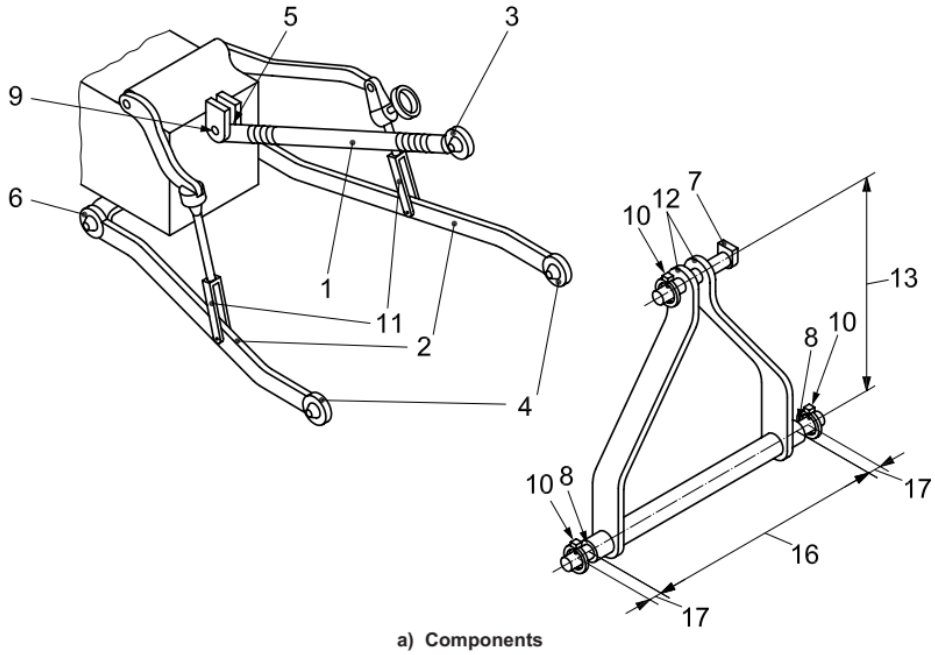

a) Components

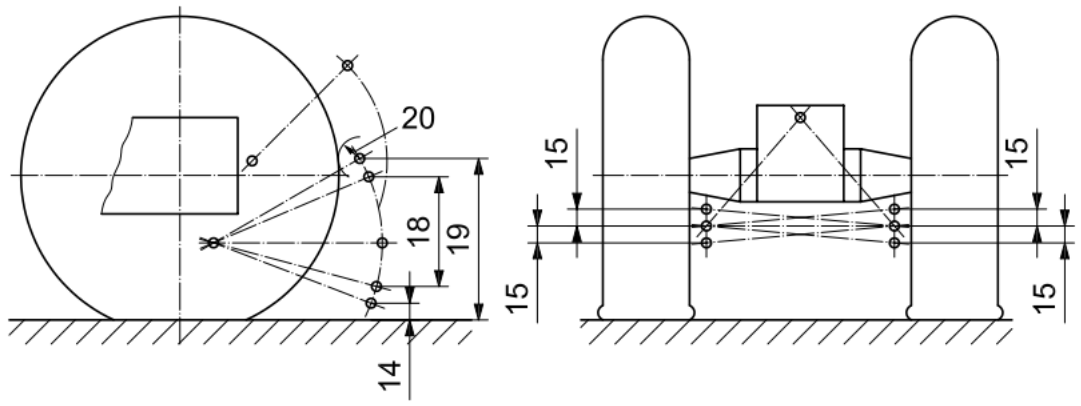

b) Dimensions

Key

1	upper link	8	lower hitch attachment	15	levelling adjustment
2	lower link	9	upper link attachment	16	lower hitch point span
3	upper hitch point	10	linchpin	17	linchpin hole distance
4	lower hitch point	11	lift rods	18	movement range
5	upper link point	12	mast	19	transport height
6	lower link point	13	mast height	20	lower hitch point clearance
7	upper hitch attachment	14	lower hitch point height		

Figure 1.2 TPH design from the ISO-730 standard a) Components and b) Dimensions (ISO, 2009).

A different approach is to consider the TPH as a six-bar mechanism that can be designed and modeled as two distinct four-bar linkages sharing two links as shown in Figure 1.3 (Ambike & Schmiedeler, 2007; Dhruw et al., 2018; Prasanna Kumar, 2012).

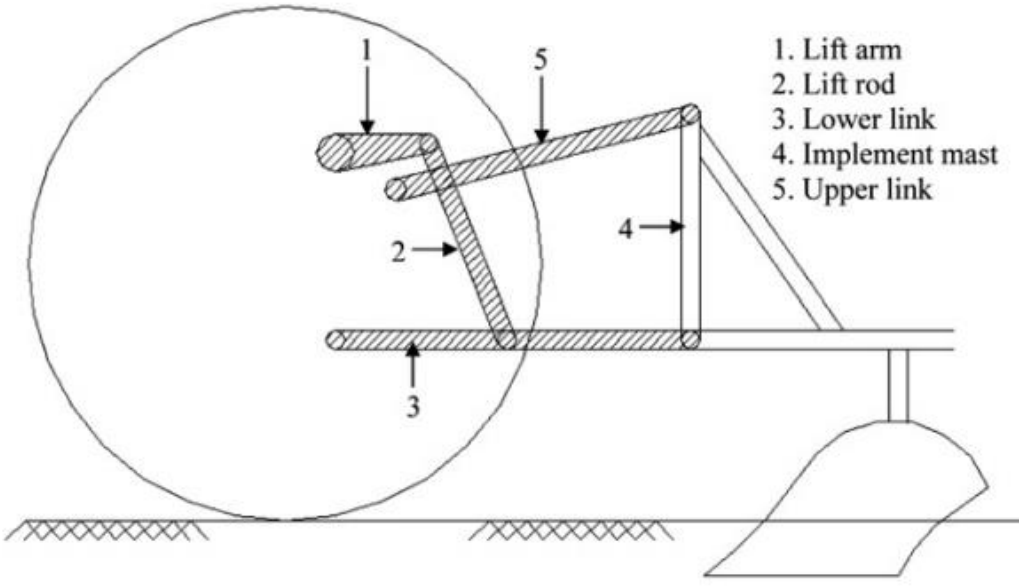

Figure 1.3 TPH modeled as a six-bar mechanism from (Prasanna Kumar, 2012).

Alternatively, Molari et al. (2014) on their study, considered the mechanism symmetrical about the plane of the tractor and for the position and static force analysis, the mechanism was divided into three kinematic subsystems: **1.** Triangle composed by tractor frame, lift arm and hydraulic cylinder; **2.** Quadrilateral composed by tractor frame, lift arm, lift rod, lower arm; **3.** Quadrilateral composed by tractor frame, upper arm, mast, lower arm (Figure 1.4).

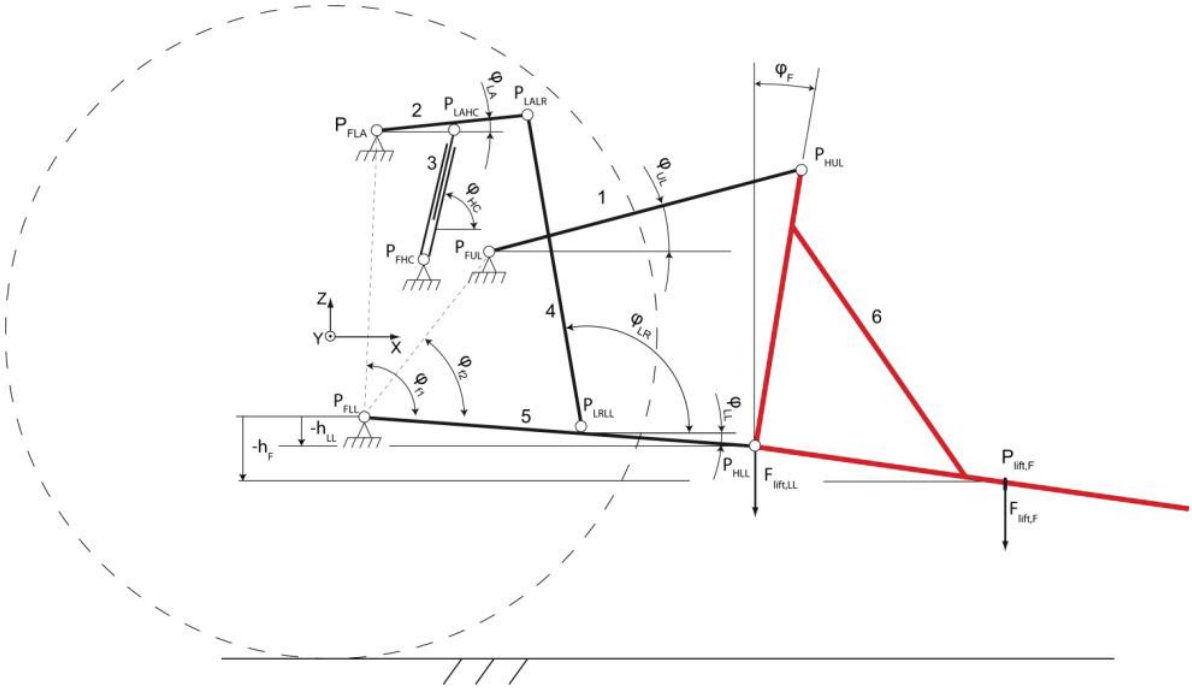

Figure 1.4 Kinematic design of the TPH from (Molari et al., 2014).

1.4 Three-Point Hitch Geometry Optimization. Literature Review

Considering the range of variation of the TPH geometrical dimensions and the requirements prescribed by ISO (2009) mechanical engineers are faced with the task of designing the TPH geometry in order to meet several kinematic, functional, structural, working, and economical requirements (Johansson, 2008; Morling, 1979).

Many attempts have been made toward TPH geometry optimization to achieve specific design requirements. Ambike and Schmiedeler (2007) proposed the application of Geometric Constraint Programming (GCP) for the determination of kinematics TPH configurations that satisfy the constraints imposed by the ASAE Standard S217.12. The design tool developed in their study also allows the user to graphically visualize the effects of the different parameters on the resulting design geometry through CAD package software. Their approach

can be easily extended to include the geometry of the tractor and to incorporate additional constraints based on the shape and size of a specific tractor model.

Prasanna Kumar (2012) developed a Newton-Raphson based algorithm capable of generating the trajectory of the lower, the upper, and the virtual hitch points. The algorithm also determines the geometric performance parameters of the TPH and its mechanical advantage, expressed in terms of the ratio of the output force to the input force of the mechanism. The algorithm was run on a group of 165 different TPHs collected from Nebraska tractor test reports and, albeit no objective functions were formally defined, optimal designs were selected based on the kinematic performance parameters and the maximum mechanical advantage of the TPH.

Kumar et al. (2018) developed a computer program that locates the virtual hitch point (VHP) of the tractor with respect to the depth of operation. The program ultimately optimizes the TPH geometry by making the VHP lie on the line of pull. Their algorithm found the locus of the VHP with respect to the depth of operation following a parabolic shape. After the iteration procedure, an increase in the distance of VHP from the rear axle center was observed when increasing the depth of operation. The most influential TPH and implement parameters on the depth of operation were the lower link length, the lower link position and the weight and height of the hitch point.

In a similar fashion, Dhruw et al. (2018) developed a design tool in which the mechanical advantage of the mechanism (ratio of the amount of vertical load on the lower hitch point to the force on the lift rod) acted as the performance parameter of the TPH. The design was established to respect the ISO-730 standard. As result, they observed that the lift rod length was the parameter that most affected the mechanical advantage, thus affecting the TPH performance. The program is simple and could be used for educational and research purposes.

Molari et al. (2014) proposed a design methodology based on a constrained optimization technique where the objective function to be maximized was related to the TPH lifting performance as defined by the OECD Code 2 (OECD, 2012). Constraints to the optimization were provided by the ISO-730 Standard requirements (ISO, 2009). As result, their program found an optimized TPH geometry that increase the lifting force by 25%. The lift arm length,

the lower link length, and their pivot point positions were the TPH parameters observed with the greatest influence on the TPH lifting performance.

1.5 Tractor-Implement Modeling

Mathematical modeling and computer simulation of the tractor-implement system allows designers to estimate dynamic loads exerted by the implement on the tractor under various operating conditions (Collins, 1991; Macmillan, 2003). However, different levels of model's accuracy could be obtained depending on the research objectives and the model's applicability (Kim & Rehkugler, 1987; Pearson & Bevly, 2007).

The quarter-vehicle model, half-vehicle model, and full-vehicle model, as shown in Figure 1.5. These models have been the most widely used for the prediction of the dynamic behavior of agricultural tractors on the vertical longitudinal plane. Depending on the model, the tractor can be represented in different manners, from a material point to a multibody object with several degrees of freedom (DOF) depending on the number of components being modeled and the simplifying assumptions being made.

However, in the case of modern agricultural tractors, the front axle is typically equipped with a suspension system while the rear axle is rigidly connected to the tractor body. In this case, the two-dimensional half-vehicle model is generally representative of the pitch motion and vertical motion of the tractor body, including the vertical motion of the front and rear wheels. Consequently the dynamic load distribution can be simulated (Gobbi et al., 2014; Previati et al., 2007; Rabbani et al., 2011; Zheng, Cui, et al., 2019; Zheng, Zhong, et al., 2019). Generally, Newton’s Second Law of Motion is then considered for the analysis of the dynamic behavior of the tractor and the implement systems.

Considerable research on the potential of tractor dynamic modeling has been carried out, mainly to evaluate tractors' overall performance, ride comfort and safety and stability reasons (Ahmadi, 2011; Gobbi et al., 2014; Guzzomi, 2012; Kim & Rehkugler, 1987; Li et al., 2015; Previati et al., 2007; Qin et al., 2019); however, less attention has been devoted to the modeling of the tractor-implement as a compound system since it implies a more complex analysis where the external forces coming from the implement can be predicted and evaluated

for different purposes (Grečenko, 1968; Macmillan, 2003; Zheng, Cui, et al., 2019; Zheng, Zhong, et al., 2019).

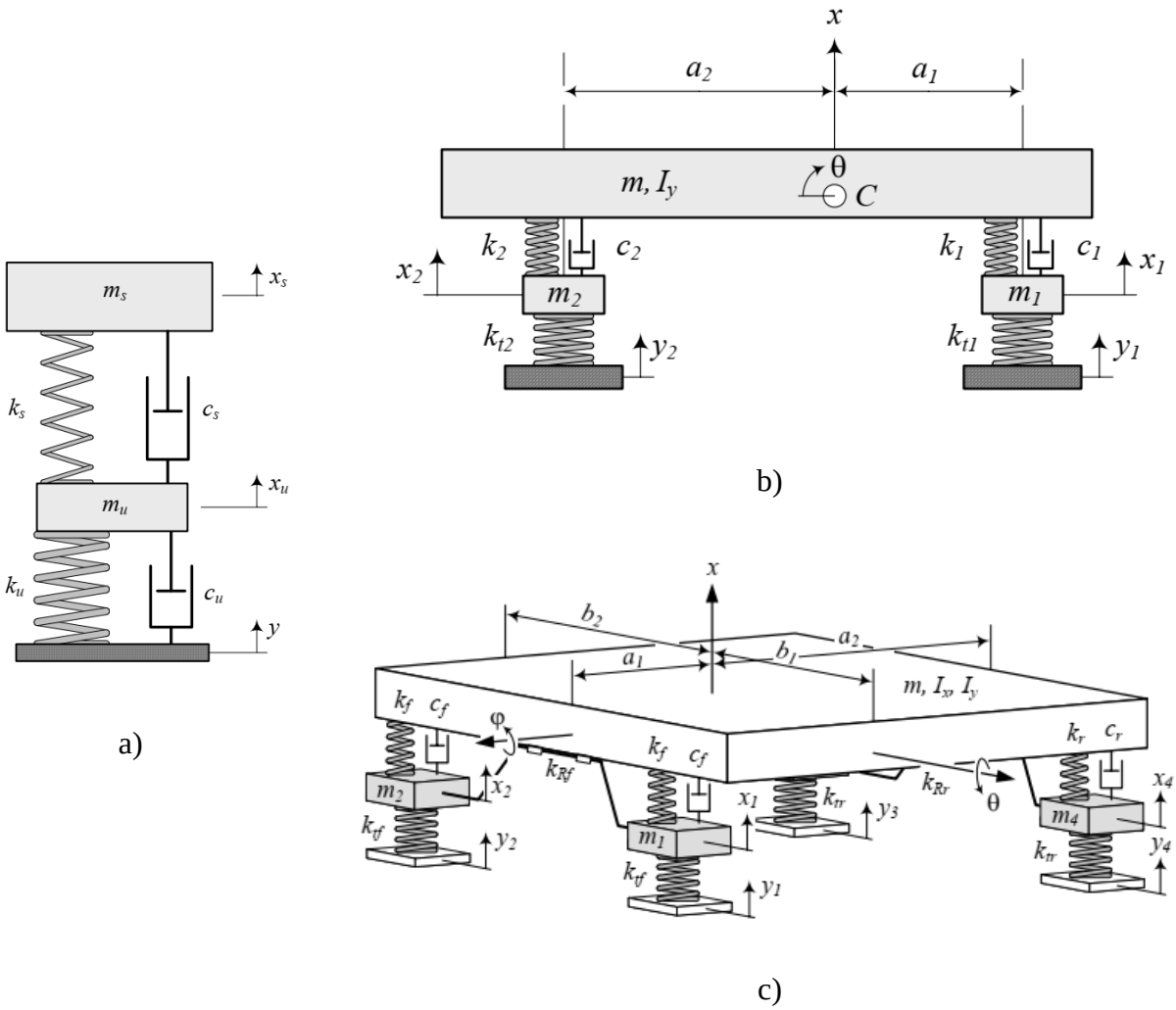

Figure 1.5 a) Quarter car model with two DOF; b) Half vehicle model-at least 3DOF; c) Full vehicle model (seven or more DOF) (Jazar, 2017).

1.5.1 Weight Transfer

The weight-transfer effect refers to the changes in the front and rear wheel reactions occurring during tractor's typical operations as a result of the ground and implement forces action on the tractor chassis. The distribution of loads on the front and rear wheel axles of tractors can directly affect the maximum traction generated by the drive wheels. Under good tractive conditions, traction increased with an increase in dynamic load. Wheel's vertical loads are proportional to the maximum traction force generated; therefore, high wheel loads are desirable from this perspective (Bauer et al., 2017; Macmillan, 2003; Oberhaus et al.,

2005). The hitching system is responsible for transmitting both vertical and horizontal forces coming from the soil-implement interaction to the tractor body; hence, the analysis of the vertical longitudinal plane is of special interest when analyzing load transfer effects. A well-mounted implement should produce the maximum possible amount of load transfer to the tractor's driving wheels, thus improving tractive performance and safety field operations (Macmillan, 2003; Srivastava et al., 2006).

An analysis for the basic understanding of weight-transfer effects under the assumption of steady state operation is well explained by Macmillan (2003), considering the tractor as composed of two rigid bodies: the drive wheels and the chassis of the tractors, as evidenced in Figure 1.6 for a rear wheel drive tractor on a slope. However, in some simple cases, it is sufficient to consider the whole tractor as a rigid body, then, the external forces are known by the weight on the wheels.

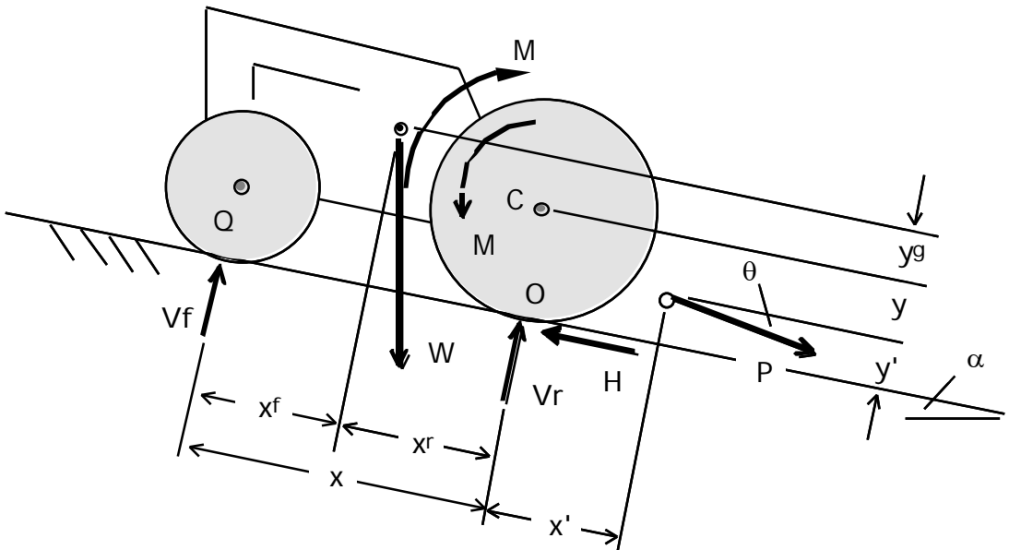

Figure 1.6 Tractor force diagram for weigh transfer analysis (Macmillan, 2003).

In this case the implement force is applied at a single point P acting through the coordinate point (x', y') at an angle θ respecting the ground surface. Then, taking the sum of the moments acting on the driving wheel and tractor body the vertical forces $V_f; V_r$ can be obtained as described in the following expression:

$$V_f = W_f - W \sin\alpha \frac{r + y_g}{x} - P \cos\theta \frac{y'}{x} - P \sin\theta \frac{x'}{x} \qquad \text{Eq. 1.1}$$

$$V_r = W_r + W \sin\alpha \frac{r + y_g}{x} + P \cos\theta \frac{y'}{x} + P \sin\theta \frac{x + x'}{x} \quad \text{Eq. 1.2}$$

Where: $W_f; W_r$ are the static weights on the wheel when the tractor is on slope (α); r is the rear wheel radio. As defined by Macmillan (2003) from the previous expressions Eq. 1.1 and Eq. 1.2, the weight transfer due to the implement can be identify from the following terms:

- $P \cos\theta \frac{y'}{x}$ is the moment effect of the implement force component down the slope decreasing the front wheel weight and increasing the rear wheel weight.
- $P \sin\theta \frac{x'}{x}$ is the moment effect of the implement force component perpendicular to the slope, decreasing the front wheel weight.
- $P \sin\theta \frac{x+x'}{x}$ is the sum of the direct moment from the implement: $P \sin\theta$, and the moment effect $P \sin\theta \frac{x'}{x}$ of the implement force component perperdicular to the slope.

Excessive weight transfer from the front to the rear tractor axle can occur during operation or maneuvering of implements connected to the tractor through the TPH. Hence, the proper design of the hitching system is fundamental to relate geometrical proportions and imposed implement loads on the tractor.

1.5.2 Soil-Implement Forces

Knowledge of the load exchange occurring between the soil and the implement during laboring is necessary to understand and predict how the load can be transferred in an effective manner through the TPH. An increasing number of studies on the modeling of the soil-implement forces have proven that these forces generated in the implement depend on physical soil properties; geometric parameters of the implement: mainly depth/width ratio (d/w) and rake angle of the tool (Figure 1.7-a); and implement operating parameters such as depth of operation, forward speed and the form of soil disturbance pattern produced by the tool. Generally, these forces are represented in a rearward and downward direction which are equivalent to the draft of the tool, and a vertical force proportional to the speed of extraction/penetration of the anchors respectively. However, some authors demonstrate experimentally that implements with rake angles over approximately 70° will change the direction of the vertical force upwards (Figure 1.7-b) (Godwin & Spoor, 1977; Payne, 1956; Payne & Tanner, 1959).

The vast majority of the existing prediction models of the implement forces are based on the principles of Mohr-Coulomb soil mechanics and on Newtonian dynamics (Godwin, 2007; Godwin et al., 2007; Godwin & Wheeler, 1996; Ibrahmi, Bentaher, Hamza, et al., 2015; McKyes, 1985; Morling, 1979). Godwin and Wheeler (1996) reported the effect of speed up to 20 km/h for tillage tine of width of 30mm and a depth of 25mm. From their experiments, forces measurements seem barely deviated from a linear relation with respect to speed (Figure 1.8).

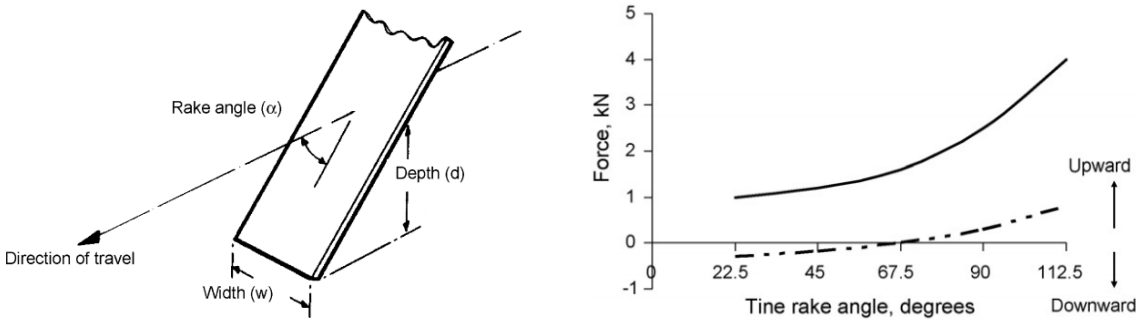

a) b)

Figure 1.7 a) Geometric parameters of the implement on the evaluation of the soil-implement forces. b) Effect of tine rake angle on horizontal (solid) and vertical (broken) forces (Godwin & O'Dogherty, 2007).

In their study Saunders et al. (2000) demonstrate that depth of operation has the greatest effect increasing the draught force by 76% when was increased from 125 mm to 225 mm; while increasing the speed from 4.5 km/h to 10 km/h increased the force form 11% and 21% at depths of 225 mm and 125 mm, respectively.

Furthermore, other researchers have reported studies about the modeling of soil-tool interaction using numerical approaches such as Finite Element Method (FEM); Discrete Element Method (DEM) (Ibrahmi, Bentaher, Hamza, et al., 2015; Shmulevich, 2010). As result, they reported a non-linear exponential relationship between draught force and working depth, while for vertical and lateral forces linear variations with the working depth were found. The three force components were found to increase linearly with speed. Cutting, and lifting angles on the forces and soil disturbance were also evaluated.

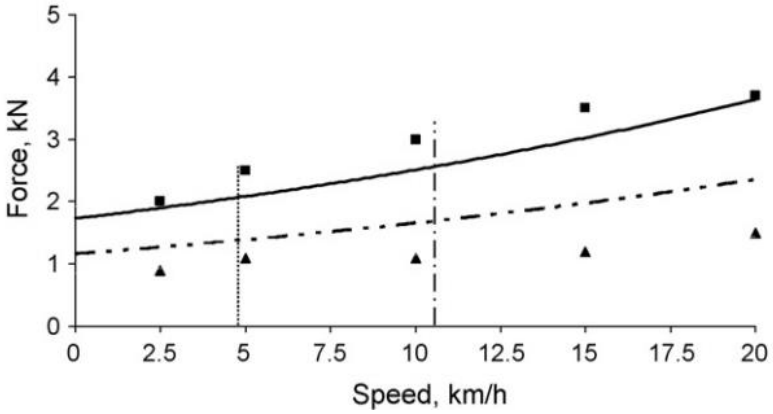

Figure 1.8 Effect of tine speed on the measure and predicted horizontal and vertical forces acting on a 40° rake angle,30mm wide,250mm deep tine on frictional soil. Horizontal force measured (■) and predicted (─). Vertical force (▲) and (--) predicted (Godwin & Wheeler, 1996).

1.6 Tractor-TPH-Implement Modeling. Literature Review

Several authors have published their research advances on the modeling and simulation of agricultural tractors. Zheng, Cui, et al. (2019) developed a dynamic model of half agricultural wheeled tractor/implement system to analyze the effects of the TPH structure, passive silent blocks of cabin, and front axle hydropneumatic suspension on the vibrational characteristics and driver comfort of the tractor system. For that purpose, they compared and evaluated the experimental and the predicted root mean square (RMS) of vertical vibration acceleration and the frequency-weighted acceleration in the time domain for the tractor dynamic models under different forward speeds, considering four main cases: (I) without cabin, front axle suspension, and implement, (II) with cabin suspension and without front axle suspension and implement, (III) with cabin suspension and implement and without front axle suspension, and (IV) with cabin, front axle suspension, and implement. As result, they observed that the driver's comfortableness will be increased due to the implement, but handling stability will be compromised.

A similar investigation was performed by Zheng, Zhong, et al. (2019), but using a complete three-dimensional multibody dynamic model of the wheeled tractor/implement system. The authors found that the presence of the implement will raise the riding comfort of drivers and the pitch stability of tractors, but dramatically worsen the roll stability.

Bauer et al. (2017) and Porteš et al. (2013) developed a model to investigate the effect of the TPH setup on the load distribution between the tractor rear wheels during in-furrow plowing. From their study, it was possible to conclude that the load difference between the in-furrow and the on-land wheels can be significantly reduced by adjusting the length of the TPH upper link. Their work highlighted the central role of the TPH in transmitting the loads acting on the implement to the tractor.

1.7 Research Problem

Albeit having provided valuable results in terms of TPH geometry optimization and tractor-implement dynamic modeling in previous sections, there are still some gaps in the literature. Investigations where the TPH geometry was subject to optimization (Ambike & Schmiedeler, 2007; Kumar et al., 2018; Molari et al., 2014), the main focus was to accomplish certain implement and hitching performance, and not to improve the overall dynamic behavior of the tractor-TPH-implement system. On the other hand, research where the dynamic performance of the aggregate tractor-TPH-implement system was considered, the influence of the TPH geometry on the transmission of the implement loads to the tractor driving axles was not studied. In addition, the proposed models are complex and highly computationally demanding leading to strong nonlinear dynamics equations (Porteš et al., 2013; Zheng, Cui, et al., 2019; Zheng, Zhong, et al., 2019).

1.8 Research Aim

The aim of the present research work is to fill the gap in the literature by developing a computational design tool ("*The Optimizer*") for the determination of an optimized TPH geometry which minimizes the weight-transfer effect, thus improving the dynamic performance of the tractor-TPH-implement system.

1.9 Research Objectives

- To define an optimization algorithm of the type constrain minimization for the TPH geometry optimization. Constraints to the minimization problem arise from the ISO-730 Standard (ISO, 2009) functional requirements and other design requirements.

- To define a reference maneuver with a reference implement and a reference soil for the simulation of the extraction of a heavy-duty implement from the soil such that the front-to-rear axle load transfer could be trigged.
- To develop a soil-implement interaction model for the simulation of the forces exerted by the soil on the implement.
- To develop a dynamic model of the aggregate system constituted by the tractor, the TPH, and the implement for the calculation of the objective function. The objective function to be minimized is defined as the tractor front-to-rear axle load transfer.
- To conduct a benchmark test that enables the analysis and discussion of the results for the evaluation of the Optimizer design tool performance.

CHAPTER 2. MATERIALS AND METHODS

The fundamentals of the Optimizer design tool are described in this chapter. For the evaluation of the influence of the TPH geometry on the weight-transfer effect, a model of an agricultural tractor equipped with a front axle suspension and bearing an implement mounted on the rear TPH is developed. A reference maneuver performed with a reference implement on a reference soil is specified to reproduce the load change during typical field operations of tractors. The loads resulting from the interaction between the implement and the soil are also estimated through the development of a soil-implement interaction model. The equations conforming the model of the tractor-TPH-implement aggregate are described. Finally, the TPH design constraints, the mathematic problem, and the solution algorithm conforming the design tool are explained.

2.1 General Structure of the Optimizer Design Tool

The general structure of the Optimizer tool is depicted in the Scheme I (Figure 2.1). The Optimizer kernel is constituted by a constrained minimization algorithm. The inputs of the Optimizer are the parameters of the tractor equipped with the TPH subject to optimization, the TPH category and its initial geometry. The optimization process is iterative, with the algorithm evaluating a trial TPH geometry (referred to as the *current TPH geometry*) at each step of the iteration. The evaluation is carried out through the tractor-TPH-implement model and consists in simulating a prescribed maneuver (referred to as the *reference maneuver*) performed with a *reference implement* while the tractor is running over a *reference soil*. The simulation allows to determine, for the current TPH geometry, the load on the tractor front

axle as a function of time and, ultimately, to extract a measure of the weight transfer during the reference maneuver, which acts as the objective function associated to the current TPH geometry. The iterative optimization process ends when a TPH geometry that minimizes the objective function is found. Such optimized TPH geometry is the output of the Optimizer. The determination of the objective function follows the algorithm described in detail in sections 2.2-2.6 and summarised in Scheme II (Figure 2.2).

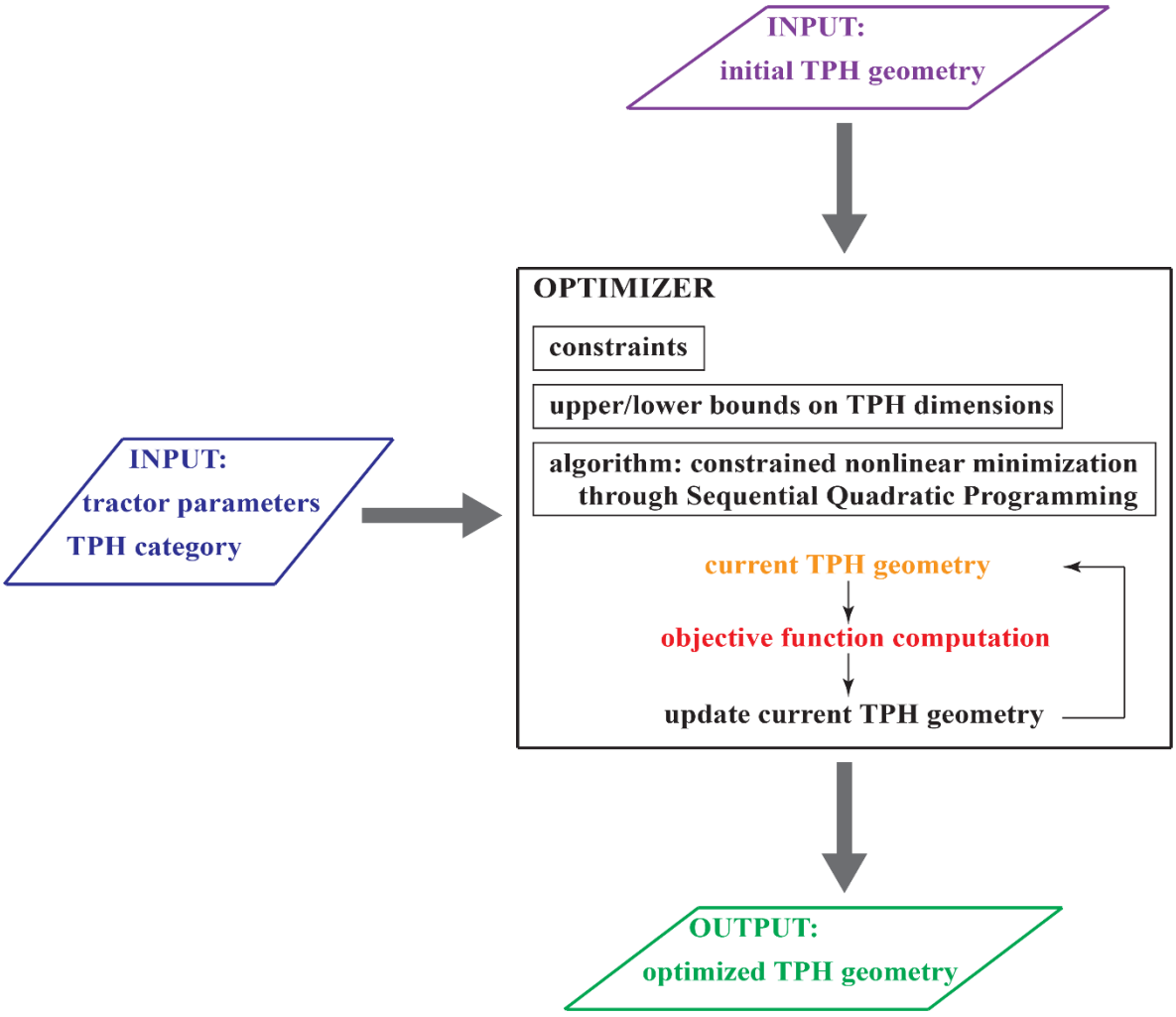

Figure 2.1 Scheme I. Optimizer workflow.

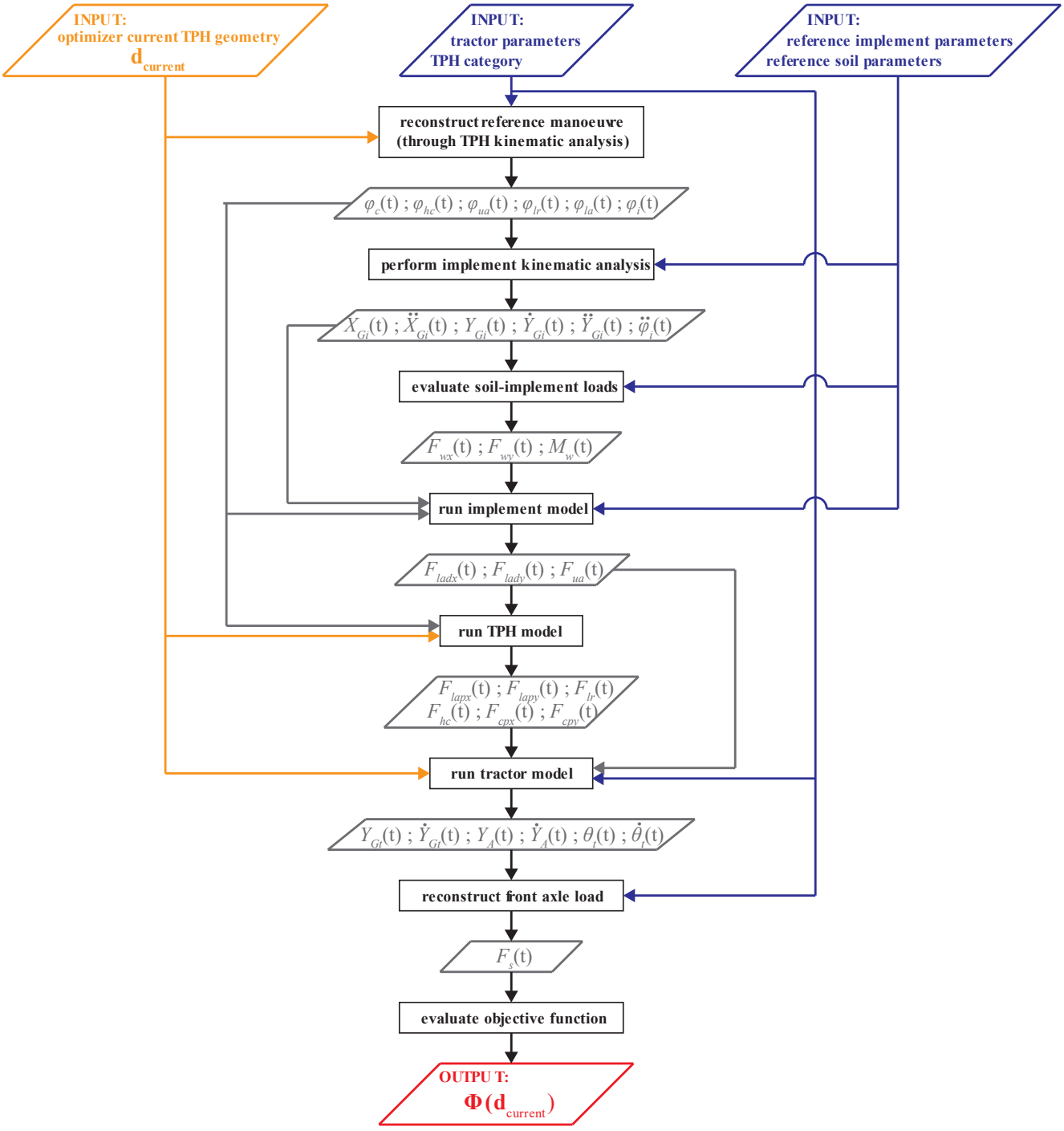

Figure 2.2 Scheme II. Algorithm for the evaluation of the objective function to be minimized by the Optimizer.

2.2 Three-Point Hitch Kinematic Analysis

Performing the kinematic analysis of the TPH is essential for simulating the reference maneuver and locating the position of the links where forces are exchanged between the implement and the TPH, and between the TPH and the tractor.

The kinematic analysis is performed in the median vertical-longitudinal plane (X-Y plane, Figure 2.3); the center of the rear axle is assumed as the origin of the reference frame. The mechanism is considered symmetrical about the X-Y plane and is divided into three subsystems: the triangle whose vertices are the points P_{hcp} , P_{hcd} , P_{cp} ; the quadrilateral whose vertices are the points P_{lap} , P_{lam} , P_{cd} , P_{cp}; and the quadrilateral whose vertices are the points P_{lap} , P_{lad} , P_{uad} , P_{uap}.

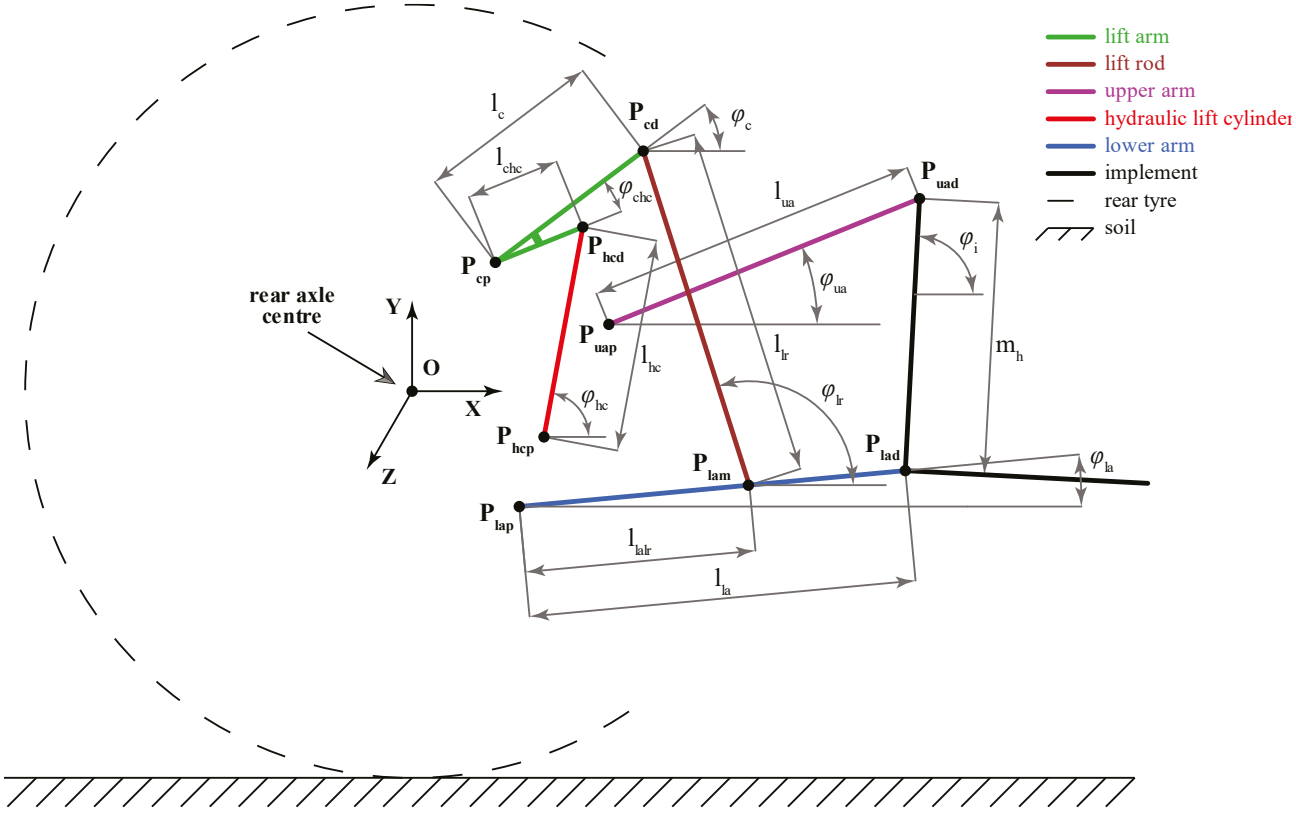

Figure 2.3 Side view of the TPH and schematic of the implement.

The analysis is based on the solution of a system of six nonlinear equations representing the condition of closure of the polygons which compose the three subsystems Eq.2.1 following the methodology proposed by Molari et al. (2014).

$$\begin{cases} X_{P_{hcp}} + l_{hc}\cos\varphi_{hc} - l_{chc}\cos\left(\varphi_c - \varphi_{chc}\right) - X_{P_{cp}} = 0 \\ Y_{P_{hcp}} + l_{hc}\sin\varphi_{hc} - l_{chc}\sin\left(\varphi_c - \varphi_{chc}\right) - Y_{P_{cp}} = 0 \\ X_{P_{cp}} + l_c\cos\varphi_c - l_{lr}\cos\varphi_{lr} - l_{lalr}\cos\varphi_{la} - X_{P_{lap}} = 0 \\ Y_{P_{cp}} + l_c\sin\varphi_c - l_{lr}\sin\varphi_{lr} - l_{lalr}\sin\varphi_{la} - Y_{P_{lap}} = 0 \\ X_{P_{uap}} + l_{ua}\cos\varphi_{ua} - m_h\cos\varphi_i - l_{la}\cos\varphi_{la} - X_{P_{lap}} = 0 \\ Y_{P_{uap}} + l_{ua}\sin\varphi_{ua} - m_h\sin\varphi_i - l_{la}\sin\varphi_{la} - Y_{P_{lap}} = 0\,. \end{cases} \quad \text{Eq. 2.1}$$

For the position analysis of the TPH to be correctly performed, the system of equations (Eq. 2.1) must have six unknowns. Depending on the specific analysis requested at the different stages of the algorithms in Scheme I and II (e.g. simulating the reference maneuver, or enforcing one of the Optimizer nonlinear constraints), the six-dimensional parameters playing the role of unknowns may vary.

2.3 Definition of the Reference Maneuver

The reference maneuver simulates the extraction of a heavy-duty implement (such as a plough or a subsoiler) from the soil and was chosen to trigger weight transfer from the front to the rear axle of the tractor. It was defined in a standardized manner, according to the dimensional requirement of the ISO-730 Standard; in this way, the maneuver is adaptable to all the TPH categories. The criteria upon which the maneuver is based are the following:

$$\begin{cases} H_{lad,min} = 1.5\,L_{14} \\ H_{lad.max} = H_{lad,min} + 0.2\,L_{18} \\ l_{lr} = l_{lr,max} \\ l_{ua}\ such\ that\ \varphi_i = \dfrac{\pi}{2}\ \text{at}\ H_{lad,min} \end{cases} \quad \text{Eq. 2.2}$$

where $H_{lad,min}$ is the minimum height of the point P_{lad} above the ground (Figure 2.4-a), $H_{lad,max}$ is the maximum height of the point P_{lad} above the ground (Figure 2.4-b), the dimensions l_{lr}, l_{ua}, φ_i are depicted in Figure 2.3, and the dimensions L_{14} and L_{18} are,

respectively, the lower hitch point height and the movement range, as defined by the ISO-730 Standard. Based on the criteria Eq. 2.2, the simulated maneuver is performed setting the lift rods at their maximum extension and the upper arm in such a way that the implement mast is vertical when the implement is at its minimum height (Figure 2.4-a). This is not a common TPH setup for real applications; however, it was defined in this way for the sake of robustness of the Optimizer: the maneuver defined in Eq. 2.2 can be successfully performed with any TPH trial geometries the Optimizer might consider during the automated optimization process.

Through the kinematic analysis of the TPH (system of equation in Eq. 2.1), the values of the hydraulic lift cylinders length when the TPH is at its lower and higher height, namely $l_{hc,min}$ and $l_{hc,max}$, are determined. Then, the speed at which the reference maneuver is performed is set by prescribing the extension law of the hydraulic lift cylinders (Figure 2.4-c) as follows:

$$l_{hc}(t) = \frac{l_{hc,max} - l_{hc,min}}{2} \cdot \mathrm{erf}\left(\frac{t - t_0}{T}\right) + \frac{l_{hc,max} + l_{hc,min}}{2} \qquad \text{Eq. 2.3}$$

where erf is the Gauss error function, T is a characteristic time to be set based on the flow rate of the hydraulic circuit actuating the hydraulic lift cylinders, t_0 is an offset time for setting the maneuver onset, and t is the simulation elapsed time. The choice of the erf function to model the cylinders extension is based on experimental observations (section 3.1).

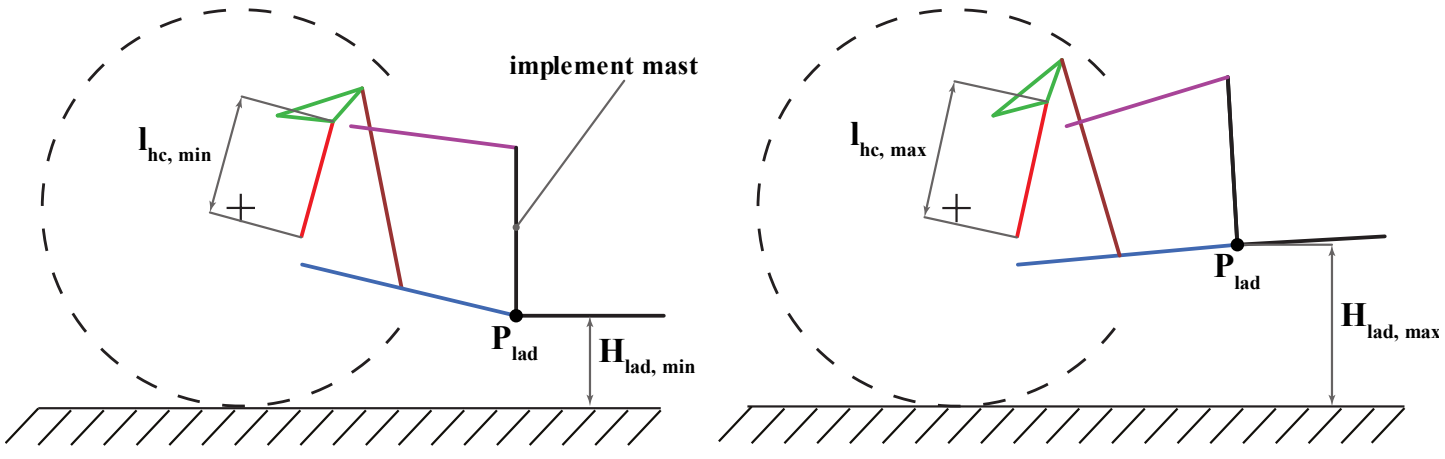

(**a**) (**b**)

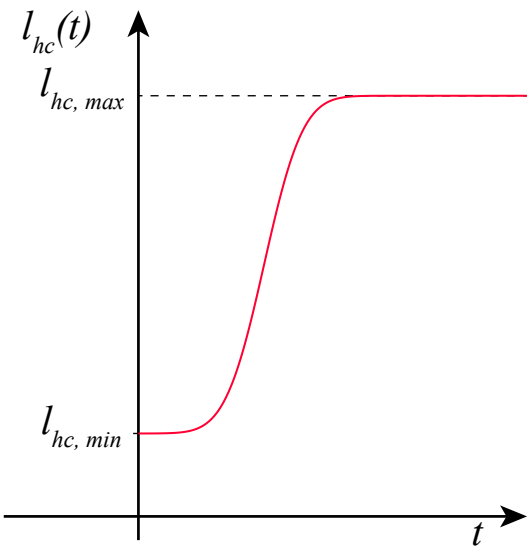

(c)

Figure 2.4 Reference maneuver: (a) TPH at lower height; (b) TPH at higher height; (c) hydraulic lift cylinders extension law.

Once the hydraulic lift cylinders extension law is set, a second kinematic analysis is performed to determine the following quantities (Scheme II):

$$\{\varphi_c(t), \varphi_{hc}(t), \varphi_{ua}(t), \varphi_{lr}(t), \varphi_{la}(t), \varphi_i(t)\}. \qquad \text{Eq. 2.4}$$

In this way, the position of each link of the TPH during the entire reference maneuver is completely known.

2.4 Implement Kinematic Analysis

Knowing, from Eq. 2.4, the values of the angles φ_{la} and φ_i, the position of the implement center of gravity (COG), G_i, can be determined:

$$\begin{cases} X_{G_i} = X_{P_{lad}} + R_i \sin(\gamma_i + \varphi_i) = X_{P_{lap}} + l_{la}\cos(\varphi_{la}) + R_i \sin(\gamma_i + \varphi_i) \\ Y_{G_i} = Y_{P_{lad}} - R_i \cos(\gamma_i + \varphi_i) = Y_{P_{lap}} + l_{la}\sin(\varphi_{la}) - R_i \cos(\gamma_i + \varphi_i) \end{cases} \qquad \text{Eq. 2.5}$$

being R_i and γ_i the polar coordinates of the implement COG with respect to point P_{lad} (Figure 2.5) and having computed the coordinates of P_{lad} according to the TPH geometry in Figure 2.3.

To complete the kinematic analysis of the implement (Scheme II), the first-order and second-order derivatives of X_{G_i}, Y_{G_i} and φ_i are computed using the central finite difference scheme.

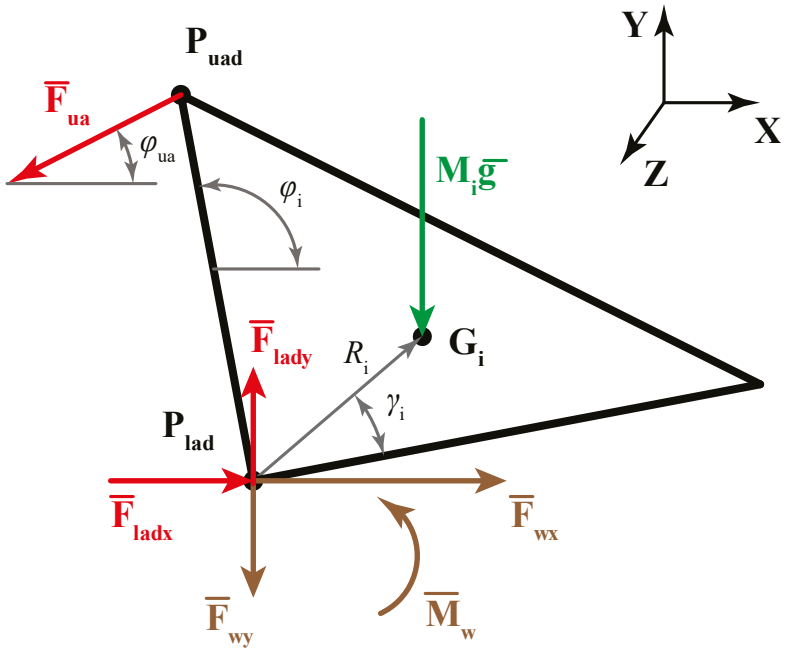

Figure 2.5 Implement model. Green line: implement weight; brown lines: soil-implement equivalent system of forces; red lines: TPH-implement forces.

2.5 Soil-Implement Interaction Model

Since the implement is assumed to behave as a rigid body, the forces exerted by the soil can be represented (Figure 2.5) as an equivalent system of forces composed by a horizontal force (F_{wx}) and a vertical force (F_{wy}) applied to a reference point of the system, plus a moment (M_w). The point P_{lad} was chosen as the reference point.

The forces exchanged between the soil and the implement depend on constitutive parameters like the geometry of the tillage tools and the soil composition and condition, as well as on operational parameters like the working depth and the tractor speed, as explained in section 3.1. Since the Optimizer simulates a reference maneuver performed with a reference implement on a reference soil, and with the tractor moving at constant speed, the forces exerted by the soil on the implement may be assumed to vary only as functions of the working depth and of the implement vertical speed, while all the other parameters remain constant. Hence, the following relations are assumed:

$$\begin{cases} F_{wx} = F_{0x} + K_{sx} \cdot Y_{P_{lad}} \\ F_{wy} = F_{0y} + K_{sy} \cdot Y_{P_{lad}} + C_{sy} \cdot \dot{Y}_{G_i} \\ M_w = M_0 + K_{sm} \cdot Y_{P_{lad}} \end{cases} \quad \text{Eq. 2.6}$$

where F_{0x}, F_{0y} and M_0 are offset values accounting for the fact that $Y_{P_{lad}}$ is not zero when the implement tools approach the soil, while K_{sx}, K_{sy} and K_{sm} are proportionality coefficients and C_{sy} is a viscous coefficient defined in Eq.2.7, in order to account for the fact that soil drag between implement penetration and extraction is different. The exact values of the coefficients appearing in Eq. 2.6-2.7 were determined at the model validation stage (section 3.1).

$$C_{sy} = \begin{cases} C_{sy}^{-}, \text{if } \dot{Y}_{G_i} \leq 0 \\ C_{sy}^{+}, \text{if } \dot{Y}_{G_i} > 0 \end{cases} \quad \text{Eq. 2.7}$$

Many studies report a nonlinear dependence of the soil loads on the working depth (Godwin, 2007; Hettiaratchi & Reece, 1974; Ibrahmi, Bentaher, Hamza, et al., 2015; Ibrahmi, Bentaher, Hbaieb, et al., 2015); however, for the sake of simplicity and without loss of generality, a linear dependence is chosen here.

2.6 Tractor-TPH-Implement Model

2.6.1 Implement Model

The equations of motion for the implement (Figure 2.5):

$$\begin{cases} F_{ladx} - F_{ua}\cos(\varphi_{ua}) + F_{wx} - M_i\,\ddot{X}_{G_i} = 0 \\ F_{lady} - F_{ua}\,\sin(\varphi_{ua}) - F_{wy} - M_i\,g - M_i\,\ddot{Y}_{G_i} = 0 \\ -F_{ladx}\,R_i\,\cos(\varphi_i + \gamma_i) - F_{lady}\,\mathrm{R_i}\,\sin(\varphi_i + \gamma_i) \\ \qquad +F_{ua}[m_h\,\sin(\varphi_i - \varphi_{ua}) + R_i\,\cos(\varphi_i - \varphi_{ua} + \gamma_i)] + M_w \\ \qquad -F_{wx}\,R_i\cos(\varphi_i + \gamma_i) + F_{wy}\,\mathrm{R_i}\,\sin(\varphi_i + \gamma_i) - I_i^{Gz}\,\ddot{\alpha}_i = 0 \end{cases} \quad \text{Eq. 2.8}$$

where F_{ua} is the force exerted by the TPH upper arm on the implement, F_{ladx} and F_{lady} are, respectively, the horizontal and vertical components of the forces exchanged by the implement and the TPH at the two lower hitch points, M_i is the implement mass, and I_i^{Gz} its moment of inertia with respect to an axis parallel to Z and passing through G_i (Figure 2.5). g is the gravitational acceleration. Note that the force F_{ua} lies in the same direction as the upper arm.

Once the kinematic analysis of the implement has been performed and the soil-implement loads have been computed, the values of F_{ladx} , F_{ladx} and F_{ua} as functions of time during the entire reference maneuver are determined from the system of equations (Eq. 2.8) (Scheme II).

2.6.2 Three-Point Hitch Model

As regards the TPH model, it is sufficient to write equilibrium equations for the lower arms (Figure 2.6-a) and for the lift arms (Figure 2.6-b), as inertial effects of the TPH links have been neglected:

$$\begin{cases} F_{lapx} + F_{lr}\cos(\varphi_{lr}) - F_{ladx} = 0 \\ F_{lapy} + F_{lr}\sin(\varphi_{lr}) - F_{lady} = 0 \\ F_{lr}\, l_{lalr}\sin(\varphi_{lr} - \varphi_{la}) - F_{lady}\, l_{la}\cos(\varphi_{la}) + F_{ladx}\, l_{la}\sin(\varphi_{la}) = 0 \end{cases} \qquad \text{Eq. 2.9}$$

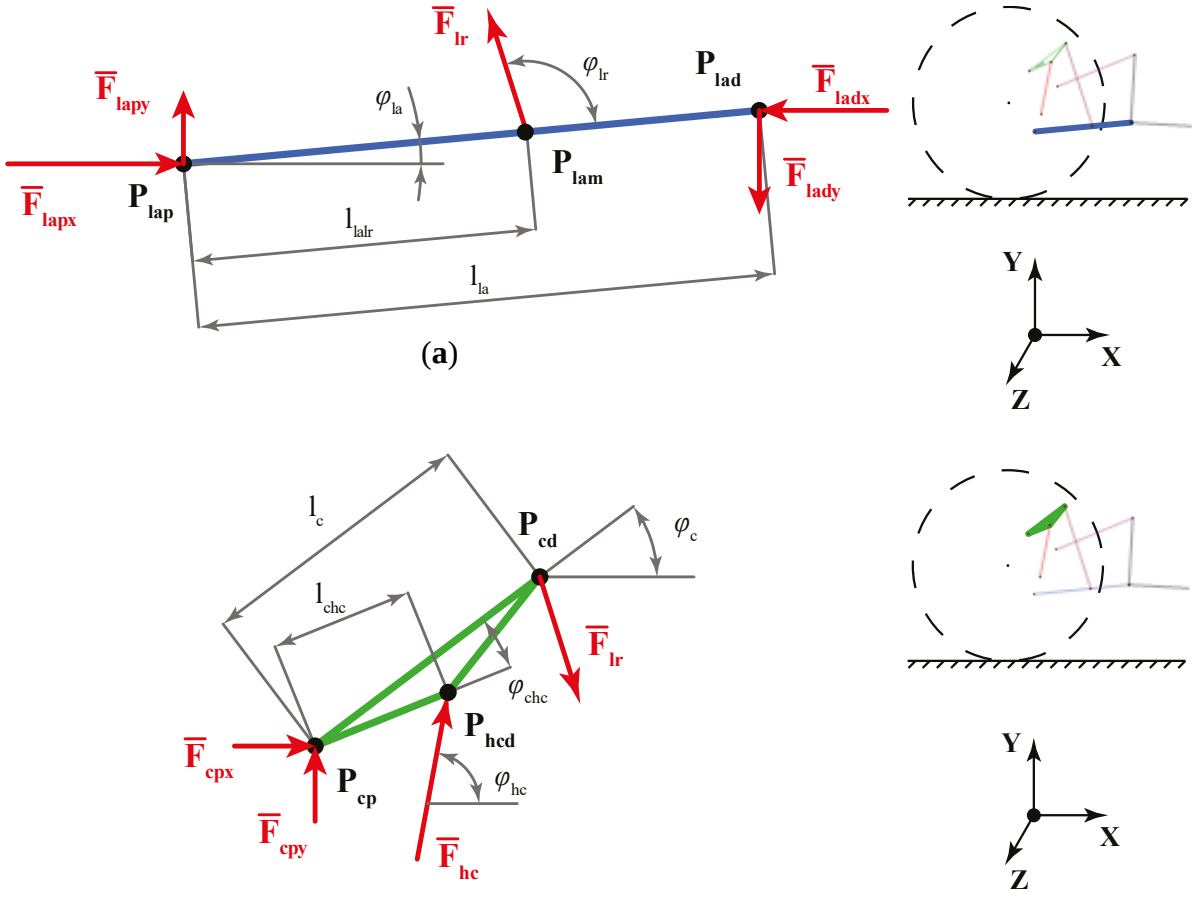

Figure 2.6 TPH model. (a) lower arms; (b) lift arms.

where F_{lapx} and F_{lapy} are, respectively, the horizontal and vertical components of the force that the tractor exerts on the TPH through the two lower link points, and F_{lr} is the force acting on the two lower arms due to the lift rods. The force F_{lr} lies in the same direction as the lift rods, and the inclination of the lift rods in the vertical-transversal plane (Y-Z plane, Figure 2.3) has been neglected for simplicity.

The equilibrium equations of the lift arms read:

$$\begin{cases} F_{cpx} + F_{hc}\cos(\varphi_{hc}) - F_{lr}\cos(\varphi_{lr}) = 0 \\ F_{cpy} + F_{hc}\sin(\varphi_{hc}) - F_{lr}\sin(\varphi_{lr}) = 0 \\ F_{hc}\, l_{chc}\sin(\varphi_{hc} - \varphi_c + \varphi_{chc}) - F_{lr}\, l_c \sin(\varphi_{lr} - \varphi_c) = 0 \end{cases} \quad \text{Eq. 2.10}$$

where F_{cpx} and F_{cpy} are, respectively, the horizontal and vertical components of the force that the tractor exerts on the TPH through the two lift arm link points, and F_{hc} is the force exerted by the two hydraulic lift cylinders on the TPH, lying on the direction of the cylinders. From the systems of equations (Eq. 2.9-2.10), the forces F_{lapx} , F_{lapy}, F_{lr}, F_{cpx}, F_{cpy} and F_{hc} as functions of time during the entire reference maneuver can be calculated (Scheme II).

2.6.3 Tractor Models

The tractor was considered equipped with a front axle suspension and bearing an implement mounted on the rear TPH. Two models were developed: a quasi-static model and a 3-DOF dynamic model. The objective was to reproduce the change on the tractor front axle load during a typical field operation while developing a mathematical model as simple as possible to speed up numerical calculations of the computational tool; nevertheless, all the features responsible for describing the weight transfer effect were included. In this sense, the following assumptions were made:

- the tractor is modelled as a system constituted by the tractor chassis and the front axle;
- the tractor chassis, the rear axle, each TPH link, and the implement behave as rigid bodies;
- friction at the TPH joints can be neglected;
- the tractor chassis, the rear axle, each TPH link, and the implement behave as rigid bodies;

- the ground surface is assumed to be horizontal;
- friction at the TPH joints can be neglected;
- the tractor performs the reference maneuver while moving forward on a straight line at constant speed.

As first alternative, a quasi-static tractor model was considered to simulate the front axle load for the Optimizer tool, since its simpler, requires only basic dimensional vehicle information and equations are based on the equilibrium condition of static forces (Figure 2.7). Therefore, steady-state operation was assumed: although the tractor and the implement were moving, the forces are doing external work but are not causing any acceleration thus, no inertial forces are considered.

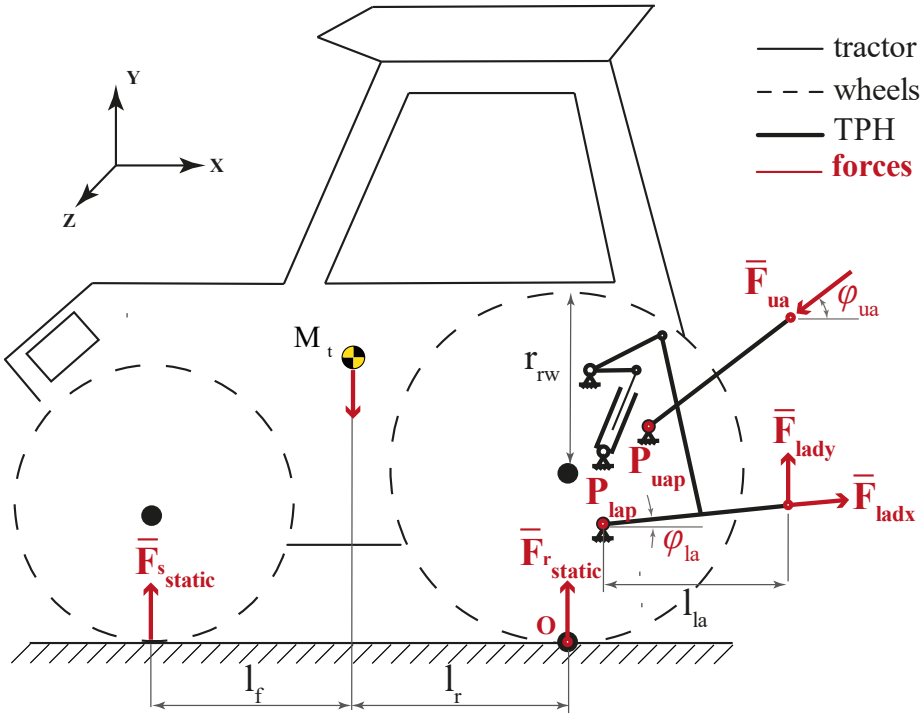

Figure 2.7 Quasi-Static tractor model

Hence, the front and rear loads acting on the tractor body are determined using planar static equilibrium equations, assuming the implement to behave as a rigid body. The forces exerted by the implement on the tractor body can be equivalent to the resulting of the forces acting on the TPH upper arm (F_{ua}) and the lower hitch points (F_{ladx}; F_{lady}). Then, the front axle load can be determined by considering the resulting moment about the point O as expressed in Eq. 2.16.

$$F_{s\,static} = \frac{1}{l_f + l_r}\left(-F_{ua}\cos\varphi_{ua}\left(Y_{P_{uap}} + r_{rw}\right) + F_{ua}\sin\varphi_{ua}\,X_{P_{uap}} + \right.$$
$$\left. -F_{lady}\left(X_{P_{lap}+}l_{la}\cos\varphi_{la}\right) + F_{ladx}\left(Y_{P_{lap}} + l_{la}\sin\varphi_{la} + r_{rw}\right) + Mtgl_r\right) \quad \text{Eq. 2.11}$$

As a second alternative, a 3-DOF dynamic model was developed, such that a more realistic simulation of the tractor motion could be obtained by considering the interactions among the mechanical components (tires, suspension springs, dampers) based on vehicle dynamics motion laws (Figure 2.8-a). Therefore, the following specific considerations were established: front and rear wheels are massless, each modelled as a linear spring and a viscous damper set in parallel between the vehicle and the ground; the front axle suspension system is modelled as a linear spring in parallel with a viscous damper. The vertical displacement of the tractor COG Y_{G_t}, the pitch angle θ_t, and vertical displacement of the front axle unsuspended mass Y_a as the degrees of freedom.

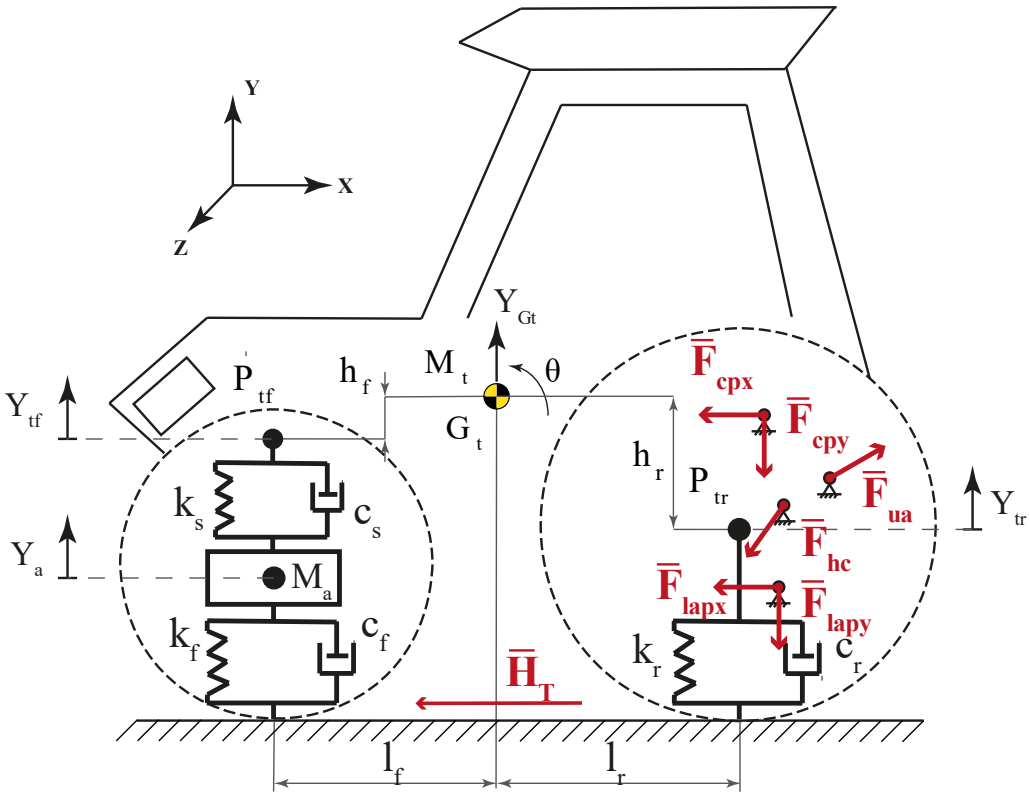

a)

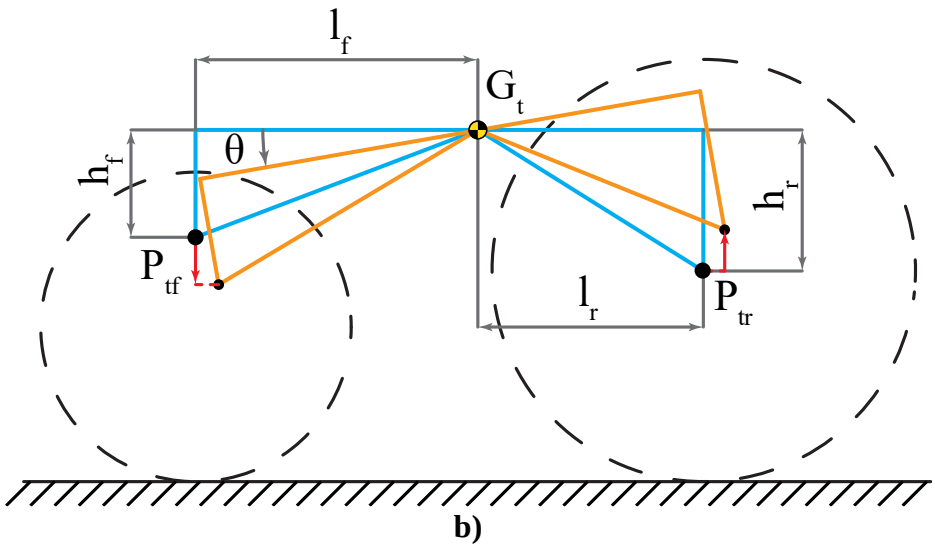

Figure 2.8 (a) The tractor model with the external loads acting on it; (b) displacement of the points P_{tf} and P_{tr} due to the sole pitch motion of the tractor.

Naming P_{tf} the link points of the front axle suspension on the tractor chassis, P_{tr} the rear wheels hub, and in accordance with the hypotheses on which the model lays, the front tyres, the rear tyres, and the front axle suspension transmit the following visco-elastic forces, respectively:

$$F_{fw} = k_f Y_a + c_f \dot{Y}_a \qquad \text{Eq. 2.12}$$

$$F_{rw} = k_r Y_{tr} + c_r \dot{Y}_{tr} \qquad \text{Eq. 2.13}$$

$$F_s = k_s(Y_{tf} - Y_a) + c_s(\dot{Y}_{tf} - \dot{Y}_a) \qquad \text{Eq. 2.14}$$

where: k_f, k_r and k_s are spring constants; c_f, c_r and c_s are damping coefficients; and Y_{tf},Y_{tr} are the vertical displacements of the points P_{tf} and P_{tr}, which can be calculated as the sum of two contributions: the displacement induced by the tractor COG vertical motion and the vertical displacement induced by the pitch motion of the tractor (Figure 2.8-b):

$$Y_{tf} = Y_{G_t} + h_f(1 - \cos\theta_t) - l_f \sin\theta_t \qquad \text{Eq. 2.15}$$

$$Y_{tr} = Y_{G_t} + h_r(1 - \cos\theta_t) + l_r \sin\theta_t \qquad \text{Eq. 2.16}$$

where h_f, h_r, l_f and l_r are the dimensions depicted in (Figure 2.8).

By taking the derivatives of Eqs. 2.15-2.16, the expressions for the vertical velocity of P_{tf} and P_{tr} are obtained:

$$\dot{Y}_{tf} = \dot{Y}_{G_t} + \dot{\theta}_t \left(h_f \sin\theta_t - l_f \cos\theta_t\right) \quad \text{Eq. 2.17}$$

$$\dot{Y}_{tr} = \dot{Y}_{G_t} + \dot{\theta}_t \left(h_r \sin\theta_t + l_r \cos\theta_t\right) \quad \text{Eq. 2.18}$$

The resulting equations of motion for the tractor model are:

$$\begin{cases} M_a\, \ddot{Y}_a = \mathrm{F_s} - \mathrm{F_{fw}} - M_a\, g \\ M_t\, \ddot{Y}_{G_t} = -F_s - F_{rw} + F_{ua} \sin\varphi_{ua} - F_{lapy} - F_{cpy} - F_{hc} \sin\varphi_{hc} - M_t\, g \\ I_t^{Gz}\, \ddot{\theta}_t = F_s\, l_f - F_{rw}\, l_r + F_{ua}\left[\left(l_r + X_{P_{uap}}\right)\sin\varphi_{ua} + \left(h_r - Y_{P_{uap}}\right)\cos\varphi_{ua}\right] + \\ \qquad -F_{cpy}\left(l_r + X_{P_{cp}}\right) - F_{cpx}\left(h_r - Y_{P_{cp}}\right) + \\ \qquad\quad -F_{hc}\left[\left(l_r + X_{P_{hcp}}\right)\sin\varphi_{hc} + \left(h_r - Y_{P_{fhc}}\right)\cos(\varphi_{hc})\right] + \\ \qquad -F_{lapy}\left(l_r + X_{P_{lap}}\right) - F_{lapx}\left(h_r - Y_{P_{lap}}\right) - H_T\left(h_r + r_{rw} + Y_{tr}\right) \end{cases} \quad \text{Eq. 2.19}$$

where M_a is the front axle unsuspended mass, M_t is the tractor chassis mass, I_t^{Gz} its moment of inertia with respect to an axis parallel to Z and passing through G_t (Figure 2.8-a), H_T is the total traction force developed at the interface between the soil and the tractor wheels, and r_{rw} is the static loaded radius of the rear wheels. As it concerns the third equation in the system (Eq. 2.19), considering the total traction force H_T is equivalent to considering the traction forces and the driving torques at the wheel hubs. However, using H_T in the calculation is easier, as there is no need to determine how traction forces and driving torques are distributed between the front and the rear wheels.

The total traction force can be determined through the balance of linear momentum of the tractor along the horizontal direction. Since the tractor is assumed to move forward on a straight line at constant speed, the acceleration of the tractor COG is null along the horizontal direction, and the balance of linear momentum reduces to an equilibrium of the horizontal components of the forces acting on the system, from which H_T can be obtained (Figure 2.8-a):

$$H_T = F_{ua}\cos\varphi_{ua} - F_{hc}\cos\varphi_{hc} - F_{lapx} - F_{cpx} \quad \text{Eq. 2.20}$$

Upon substituting Eqs. 2.11-2.13 and Eq. 2.20 into Eq. 2.19, and accounting for Eqs. 2.15-2.18, a system composed of three second-order ordinary differential equations (ODEs) is obtained, constituting the tractor model in the algorithm depicted in Scheme II. The values of the loads exerted by the TPH on the tractor during the entire reference maneuver are known

from the previous steps of the algorithm and solving the system of equations in Eqs. 2.19, allows to determine the quantities:

$$\{Y_a(t), Y_{G_t}(t), \theta_t(t)\} \qquad \text{Eq. 2.21}$$

The system of Equations Eq. 2.19 is solved using an explicit Runge-Kutta method through the MATLAB built-in function *ode45* (MATLAB®, Mathworks, Inc., MA, USA).

Once the values of the quantities in Eq. 2.21 have been determined, the load on the tractor front axle as a function of time during the entire reference maneuver can be reconstructed (Scheme II). Accounting for Eqs. 2.14-2.15 and Eq. 2.17, the front axle load takes the form:

$$\begin{aligned} F_s = k_s\big(Y_{G_t} + h_f(1-\cos\theta_t) - l_f\sin\theta_t - Y_a\big) \\ + c_s\left(\dot{Y}_{G_t} + \dot{\theta}_t\left(h_f\sin\theta_t - l_f\cos\theta_t\right) - \dot{Y}_a\right) \end{aligned} \qquad \text{Eq. 2.22}$$

Resulted front axle load obtained from both, the quasi-static tractor model, and the dynamic tractor model (Eq.2.16 and Eq. 2.22), was compared with an experimental front axle load measured during an in-filed maneuver similar to the reference maneuver performed with the subsoiler used for the validation tests (section 3.2). The feasibility of using the quasi-static model or the dynamic model on the computational tool performance is also evaluated in the section 3.2.

2.6.4 Parameter Identification of the Dynamic Tractor Model

A parameter identification procedure was performed to determine the spring, damping and inertial coefficients conforming the dynamic tractor model. The identification consisted in choosing the parameter values that best matched the higher and lower peak in the simulated front axle load with those from the experimental front axle load measured during the in-filed maneuver. The algorithm was set by defining a nonlinear unconstrained optimization problem in Eq. 2.23. The starting values for the parameter identification procedure were taken from data available in the literature (Melzi et al., 2014; Qin et al., 2019; Zheng, Cui, et al., 2019; Zheng, Zhong, et al., 2019).

The problem was solved through the MATLAB built-in function *fmincon* (MATLAB®, Mathworks, Inc., MA, USA).

$$\begin{cases} \min\limits_{w} \Psi(w) \\ L_{w\,j} \leq w_j \leq U_{w\,j}, j = 1, \cdots, N_W \end{cases} \quad \text{Eq. 2.23}$$

where w is a vector containing all the dynamic tractor model parameters, Ψ is the objective function to be minimised, $L_{w\,j}$ and $U_{w\,j}$ are, respectively, the lower and upper bounds on the dimension w_j, and N_W is the number of tractor model parameters subject to optimization. The dimensions vector is composed by $N_W = 7$ parameters, namely:

$$w = \left[k_s; k_f; k_r; c_s; c_f; c_r; I_t^{Gz}\right]$$

The objective function was defined as the sum of the quadratic errors e_p and e_v (Eq. 2.24)

$$\Psi = (e_p^2 + e_v^2) \quad \text{Eq. 2.24}$$

Where e_p is the peak error, calculated as the difference between the experimental and simulated peak and e_v is the valley error, calculated as the difference between the experimental valley and the simulated valley as defined in Eqs. 2.25-2.26. (Figure 2.9).

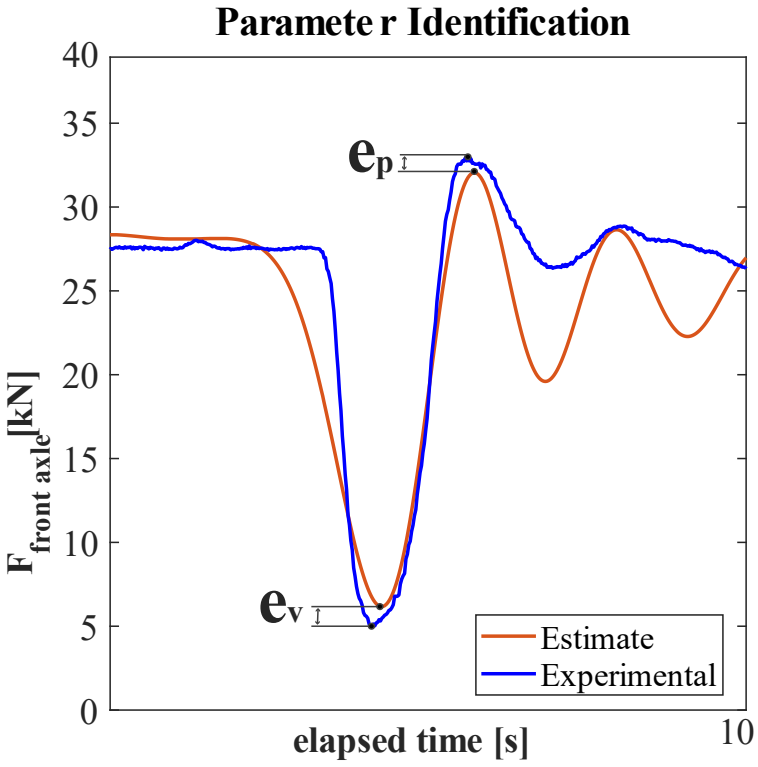

Figure 2.9 Parameter identification procedure

$$e_p = experimental_{peak} - simulated_{peak} \quad \text{Eq. 2.25}$$

$$e_v = experimental_{valley} - simulated_{valley} \quad \text{Eq. 2.26}$$

2.7 The Optimizer Design Tool

The Optimizer solves the following mathematical problem (Scheme I):

$$\begin{cases} \min\limits_{d} \Phi(d) \\ C_k(d) \leq 0, k = 1, \cdots, N_C \\ L_j \leq d_j \leq U_j, j = 1, \cdots, N_D \end{cases} \quad \text{Eq. 2.27}$$

where d is a vector containing all the TPH dimensions subject to optimisation, Φ is the objective function to be minimised, C_k are the constraints that the TPH has to satisfy, N_C is the number of constraints, L_j and U_j are, respectively, the lower and upper bounds on the dimension d_j, and N_D is the number of TPH dimensions subject to optimisation. The dimensions vector is composed by $N_D = 19$ TPH dimensions, namely:

$$d = \left[X_{P_{cp}}; Y_{P_{cp}}; X_{P_{hcp}}; Y_{P_{hcp}}; X_{P_{lap}}; Y_{P_{lap}}; X_{P_{uap}}; Y_{P_{uap}}; l_c; l_{chc}; l_{la}; l_{lalr}; l_{lr_{max}}; l_{lr_{min}}; l_{ua_{max}}; l_{ua_{min}}; \varphi_{chc}; \varphi_{c_{max}}; \varphi_{c_{min}}\right]$$

The objective function is the peak-to-peak (P2P) value of the front axle load defined in Eq. 2.28; during the reference maneuver and is determined through the algorithm depicted in Scheme II:

$$\Phi = \mathrm{P2P}(F_s) \quad \text{Eq. 2.28}$$

Ensuring that the Optimizer minimizes $\Phi(\mathrm{d})$ will result in finding the TPH optimal geometry which minimizes the weight-transfer effect during the reference maneuver. Problem in Eq. 2.27 is solved using an active-set sequential quadratic programming method through the MATLAB built-in function *fmincon* (MATLAB®, Mathworks, Inc., MA, USA).

2.7.1 Optimizer Constraints

The Optimizer accounts for $N_C = 36$ constraints (Table 1), implemented in the non-dimensional form $C_k(x) \leq 0$. For the sake of readability, constraints will not be presented in this form in Table 1, but in the form they were naturally derived.

Table 1 Optimizer constraints.

Nr.	Equation	Significance
C1	$\varphi_{c,max} \geq \varphi_{c,min}$	Logical constraints
C2	$l_{lr,max} \geq l_{lr,min}$	
C3	$l_{ua,max} \geq l_{ua,min}$	
C4	$l_c + l_{lr,min} + l_{lalr} \geq \lvert P_{lap} - P_{cp} \rvert$	Robustness constraints
C5	$l_{lr,min} + l_{lalr} + \lvert P_{lap} - P_{cp} \rvert \geq l_c$	
C6	$l_c + l_{lr,min} + \lvert P_{lap} - P_{cp} \rvert \geq l_{lalr}$	
C7	$l_c + \lvert P_{lap} - P_{cp} \rvert + l_{lalr} \geq l_{lr,max}$	
C8	$m_h + l_{la} + l_{ua,min} \geq \lvert P_{lap} - P_{uap} \rvert$	
C9	$m_h + \lvert P_{lap} - P_{uap} \rvert + l_{ua,min} \geq l_{la}$	
C10	$m_h + l_{la} + \lvert P_{lap} - P_{uap} \rvert \geq l_{ua,max}$	
C11	$l_c - l_{chc} \geq 50$ mm	Functional constraints
C12	$l_{la} - l_{lalr} \geq 200$ mm	
C13	$Y_{P_{cp}} - Y_{P_{lap}} \geq 50$ mm	
C14	$Y_{P_{uap}} - Y_{P_{lap}} \geq 300$ mm	
C15	$Y_{P_{hcp}} - Y_{P_{lap}} \geq 0$ mm	
C16	$\varphi_{hc,max} \leq 85°$	
C17	$\frac{l_{hc,min}}{l_{hc,max}} \geq 0.6$	Proportioning constraints
C18	$\frac{l_{lr,min}}{l_{lr,max}} \geq 0.7$	
C19	$\frac{l_{ua,min}}{l_{ua,max}} \geq 0.6$	
C20	$X_{P_{lap}} + l_{la} - X_{PTO} \geq L_{MIN}$	Tractor PTO distance from lower hitch points (ISO-730, Figure 2 & Table 2)
C21	$X_{P_{lap}} + l_{la} - X_{PTO} \leq L_{MAX}$	
C22	$H_{lad,min} \leq L_{14}$	Lower hitch points height, TPH in configuration A (dimension L_{14} as per ISO-730)
C23	$H_{lad,min} \geq 50$ mm	
C24	$\varphi_{lr} \geq 95°$	Functional requirements for TPH in configuration A
C25	$\varphi_i \leq 90°$	

C26	$H_{lad,max} \geq L_{19}$	Transport height, TPH in configuration B (dimension L_{19} as per ISO-730)
C27	$\Delta_{min} \geq L_{20}$	Lower hitch points clearance, TPH in configuration B (dimension L_{20} as per ISO-730)
C28	$l_{ua} \geq l_{ua,min}$	Functional constraints for configuration C
C29	$l_{ua} \leq l_{ua,max}$	
C30	$\frac{l_{lr,max} + l_{lr,min}}{2} \geq l_{lr,lim}$	
C31	$L_{CV} \geq 0.9\left(l_f + l_r\right)$	Constraints on vertical convergence distance
C32	$L_{CV} \leq 3\left(l_f + l_r\right)$	
C33	$\frac{H_{lad,max} - H_{lad,min}}{2} \geq L_{15}$	Levelling adjustment, TPH in configuration C (dimension L_{15} as per ISO-730)
C34	$H_{lad,max} - H_{lad,min} \geq L_{18}$	Movement range, TPH from configuration D_1 to D_2 (dimension L_{18} as per ISO-730)
C35	$\varphi_{i,max} \geq 95°$ (90° for category 1N TPH)	Mast adjustment, TPH in configurations E_1 and E_2 (ISO-730, comma 3.2.22)
C36	$\varphi_{i,min} \leq 85°$ (80° for category 1N TPH)	

Constraints C1-C3 are *logical constraints* on some of the elements of d: for obvious reasons, the maximum extension of the lift rods and of the upper arm cannot be less than their minimum extension; similarly, the maximum value of the lift arms angle cannot be less than its minimum value. Constraints C4-C10 are *robustness constraints*: they prescribe conditions for the existence of the closed polygons which constitute the TPH kinematic subsystems described in section 2.2**,** thus impeding the Optimizer from choosing trial geometries that would result in unfeasible TPH mechanisms. Constraints C11-C16 are *functional constraints*: for manufacturing and accessibility reasons, there needs to be a minimum ensured distance between some link points; moreover, the hydraulic lift cylinders must not reach a vertical

position when fully extended. Constraints C17-C19 are *proportioning constraints* on the ratio of minimum to maximum length of the extensible links, set to avoid disproportioning.

The other constraints are derived from the requirements contained in the ISO-730 Standard: constraints C20-C21 account for the tractor power take-off (PTO) location with respect to the TPH, while constraints C22-C36 concern the functional performance of the TPH and are enforced by evaluating, through the kinematic analysis described in section 2.2, the TPH geometry in the different configurations described in the following:

Configuration A (Figure 2.10-a)

It has the following features:

- lift rods set at maximum length: $l_{lr} = l_{lr,max}$;
- upper arm set at maximum length: $l_{ua} = l_{ua,max}$;
- hydraulic lift cylinders fully closed: $l_{hc} = l_{hc,min}$; i.e., lift arms at minimum angle: $\varphi_c = \varphi_{c,min}$.

From this configuration, the lower hitch points height above the ground $H_{lad,min}$ depicted in Figure 2.10-a is deduced, and constraints C22-23 are enforced. Constraints C24 and C25 are additional functional requirements prescribing that the lift rods must not be close to vertical position and that the implement is inclined rearward in this configuration.

Configuration B (Figure 2.10-b)

It has the following features:

- lift rods set at minimum length: $l_{lr} = l_{lr,min}$;
- upper arm set at intermediate length: $l_{ua} = \frac{l_{ua,max}+l_{ua,min}}{2}$;
- hydraulic lift cylinders fully extended: $l_{hc} = l_{hc,max}$; i.e., lift arms at maximum angle: $\varphi_c = \varphi_{c,max}$.

This configuration is used to enforce constraint C26 on the transport height $H_{lad,max}$ depicted in Figure 2.10-b and constraint C27 on the lower hitch points clearance Δ_{min}. Both the transport height and the lower hitch point clearance are defined by the ISO-730 Standard, the latter being calculated as follows:

$$\Delta_{min} = \sqrt{\left(X_{P_{lap}} + l_{la}\cos\varphi_{la}\right)^2 + \left(Y_{P_{lap}} + l_{la}\sin\varphi_{la}\right)^2} - r_{rw} \qquad \text{Eq. 2.29}$$

Configuration C (Figure 2.10-c)

It has the following features:

- lift rods set at intermediate length: $l_{lr} = \frac{l_{lr,max}+l_{lr,min}}{2}$;
- horizontal lower arms: $\varphi_{la} = 0°$;
- vertical implement mast: $\varphi_i = 90°$.

The length at which the upper arm needs to be set in configuration C is:

$$l_{ua} = \sqrt{\left(X_{P_{lap}} + l_{la} - X_{P_{uap}}\right)^2 + \left(Y_{P_{lap}} + m_h - Y_{P_{uap}}\right)^2} \qquad \text{Eq. 2.30}$$

while the minimum value of lift rod length that allows to have horizontal lower arms is:

$$l_{lr,lim} = \sqrt{\left(X_{P_{lap}} + l_{lalr} - X_{cp} - l_c\,cos\,\varphi_{c,min}\right)^2 + \left(Y_{P_{cp}} + l_c\,sin\,\varphi_{c,min} - Y_{P_{lap}}\right)^2} \qquad \text{Eq. 2.31}$$

To ensure that configuration C can be obtained, constraints C28-C30 are enforced: constraints C28 and C29 ensure that the length l_{ua} in Eq. 2.25 falls within the minimum and maximum upper arm length, while constraint C30 ensures that the intermediate lift rods length is greater than the limit value determined through Eq. 2.26.

From configuration C, the vertical convergence distance L_{CV} of the TPH (ISO-730, 2009) can be calculated by observing that:

$$\frac{L_{CV}}{X_{P_{lap}} + l_{la} - X_{P_{uap}}} = \frac{m_h}{m_h - \left(Y_{P_{uap}} - Y_{P_{lap}}\right)},$$

which leads to:

$$L_{CV} = m_h\,\frac{X_{P_{lap}} + l_{la} - X_{P_{uap}}}{m_h - Y_{P_{uap}} + Y_{P_{lap}}} \qquad \text{Eq. 2.32}$$

Once L_{CV} is determined, constraints C31 and C32 can be enforced: the former is prescribed by the ISO-730 Standard, while the latter represents an upper limit on L_{CV} and is set for design reasons.

Configuration C is also used to enforce constraint C33 on the levelling adjustment required by the ISO-730 Standard. This is done by evaluating the heights $H_{lad,min}$ and $H_{lad,max}$ of the lower hitch points above the ground (Figure 2.10-c). $H_{lad,min}$ is obtained starting from configuration C and fully extending one lift rod, while $H_{lad,max}$ is found starting from configuration C and shortening one lift rod to its minimum length.

Configuration D1 and D2 (Figure 2.10-d)

These configurations are used to enforce the constraint C34 on the movement range required by the ISO-730 Standard and are reached with the following TPH setup:

- lift rods set at intermediate length: $l_{lr} = \frac{l_{lr,max}+l_{lr,min}}{2}$;
- upper arm set at intermediate length: $l_{ua} = \frac{l_{ua,max}+l_{ua,min}}{2}$;
- configuration D1: hydraulic lift cylinders fully closed ($l_{hc} = l_{hc,min}$; $\varphi_c = \varphi_{c,min}$);
- configuration D2: hydraulic lift cylinders fully extended ($l_{hc} = l_{hc,max}$; $\varphi_c = \varphi_{c,max}$).

The kinematic analysis of the TPH in these configurations allows to determine the lower hitch point heights above the ground $H_{lad,min}$ and $H_{lad,max}$ (Figure 2.10-d) and, ultimately, the movement range as the difference between the two.

Configurations E1 and E2 (Figure 2.10-e) and (Figure 2.10-f)

These configurations are used to enforce the constraint on the mast adjustment as defined by ISO-730. The Standard sets two limit TPH configurations (by prescribing the height of the lower hitch points above the ground) and prescribes that for any configurations in between these two, the implement mast needs to range from a minimum angle of 85° with respect to the horizontal (80° for category 1N TPHs) to a maximum angle of 95° with respect to the horizontal (90° for category 1N TPHs).

From simple geometrical considerations, it emerges that the most critical configuration for meeting the requirement on the maximum mast angle is the one where the lower hitch points are the lowest, while the most critical configuration for meeting the requirement on the minimum mast angle is the other. Therefore, two configurations are set as follows:

- E1: height of lower hitch points above the ground set at the value $H_{ma,min}$ prescribed by the Standard (ISO-730, Table 3, No. 3.2.22 “lowest position”); upper arm set at minimum length: $l_{ua} = l_{ua,min}$;
- E2: height of lower hitch points above the ground set at the value $H_{ma,max}$ prescribed by the Standard (ISO-730, Table 3, No. 3.2.22 “highest position”); upper arm set at maximum length: $l_{ua} = l_{ua,max}$.

From the kinematic analysis of the TPH in configuration E1, the maximum mast angle $\varphi_{i,max}$ is determined and constraint C35 is enforced; the same analysis performed in configuration E2 allows to determine the minimum mast angle $\varphi_{i,min}$ and to enforce constraint C36.

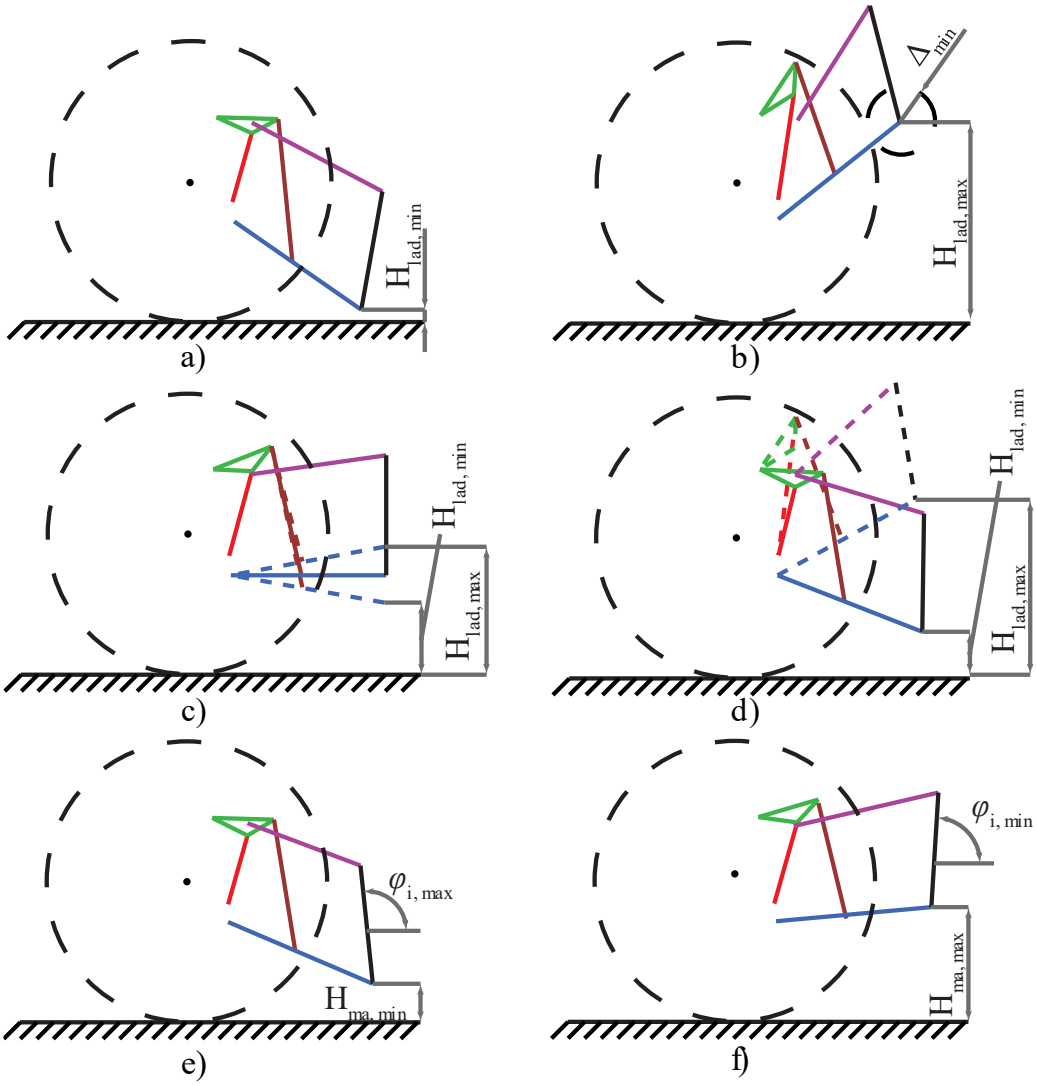

Figure 2.10 TPH configurations used to enforce constraints C22-C36 (Table 1).

CHAPTER 3. RESULTS AND DISCUSSION

The validation of the previously developed models described in the Materials and Methods (Chapter 2), is demonstrated in this Chapter. The behavior of the tractor-TPH-implement aggregate system during the defined reference maneuver is simulated and results are analyzed. The feasibility of using the quasi-static or the dynamic tractor model for the performing of the Optimizer tool is evaluated through a comparative analysis. The capabilities of the design tool were studied through a benchmark test.

3.1 Model Validation

To understand and predict the forces exchanged between the implement and the soil during tractor laboring a series of predictive models have been proposed in the literature. It has been demonstrated that these forces depend mainly on the geometric and operational implement parameters as well as on physical soil properties (section 1.3.2). In this research work a soil-implement interaction model has been developed in the previous section 2.5 (Eqs. 2.6-2.7). However, different from the existing literature models, the forces exerted by the soil on the implement have been assumed to vary only as functions of the implement working depth and on the speed of penetration/extraction of the implement into/from the soil, whereas all other parameters have been considered constant.

For the validation of the developed soil-implement interaction model and to determine the values of the coefficients in equations (Eqs. 2.6-2.7), a series of tests were conducted (Figure 3.1) in which a tractor with a sensorized TPH performed a maneuver similar to the reference maneuver described in section 2.3. Tests were performed on a clay-loam untilled soil, in a farm located in northern Italy. The tractor used for the tests was a 96 kW mechanical front wheel drive (MFWD) tractor with a rear-mounted category 3 TPH. A 7-shank subsoiler

(Table 3-1) was attached to the tractor and the loads at different locations of the TPH were measured during implement maneuvering. The tractor was equipped with the following sensors: a pressure sensor mounted on the hydraulic lift cylinders; a load cell placed on the TPH upper arm; a load cell that measured the horizontal component of the force at the lower link points; a sensor for measuring the lift arms angle with respect to the horizontal direction, which allowed to reconstruct the TPH configuration; and a pressure sensor on the front-axle hydropneumatic suspension.

Table 3-1 Implement used in the validation tests.

Implement type	subsoiler
Number of tools	7 shanks
M_i	768 kg
I_i^{Gz}	314 kg m^2
R_i	795 mm
γ_i	5.19°
m_h	690 mm

Figure 3.1 Model validation tests setup: a 7-shanks subsoiler is connected to the rear TPH of the tractor.

The maneuver consisted in raising and lowering the subsoiler while the tractor was running on untilled soil at a constant speed of 2 km/h. Several consecutive repetitions of the maneuver were performed. For the whole extent of the maneuver, the subsoiler shanks were sunk under the ground.

Figure 3.2 shows a comparison between the measured and the simulated TPH configuration in terms of the hydraulic lift cylinders extension for three test repetitions; the simulated values were determined using Eq. 2.3. It can be observed that the model is able to reproduce the experimental maneuver and, the *erf* function appears to be an effective choice for approximating the cylinder kinematics observed in the field tests.

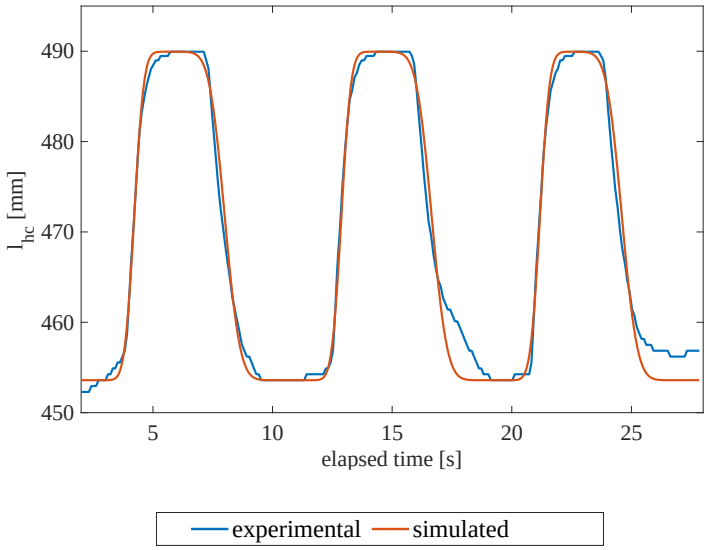

Figure 3.2 Reconstruction of the hydraulic lift cylinders extension during three maneuver repetitions.

Figure 3.3 shows a comparison between the force measured at different locations of the TPH and the force predicted through the soil-implement interaction model in equations Eqs. 2.6-2.7, the implement model in Eq. 2.8 and the TPH model in Eqs. 2.9-2.10. From the comparison, it can be concluded that the soil-implement interaction model is suitable for describing the loads that the soil exerts on the subsoiler shanks during a raising/lowering maneuver. In particular, the peak in the hydraulic lift cylinders force during implement extraction from the soil is reproduced. Further analysis show that such peak is aligned with the peak in the implement vertical speed (Figure 3.4), suggesting that the loads exerted by the soil on the implement should depend not only on the working depth, but also on the speed

of penetration/extraction of the implement into/from the soil. This is the reason that led to the introduction of the viscous term in the expression of F_{wy} in Eq. 2.6.

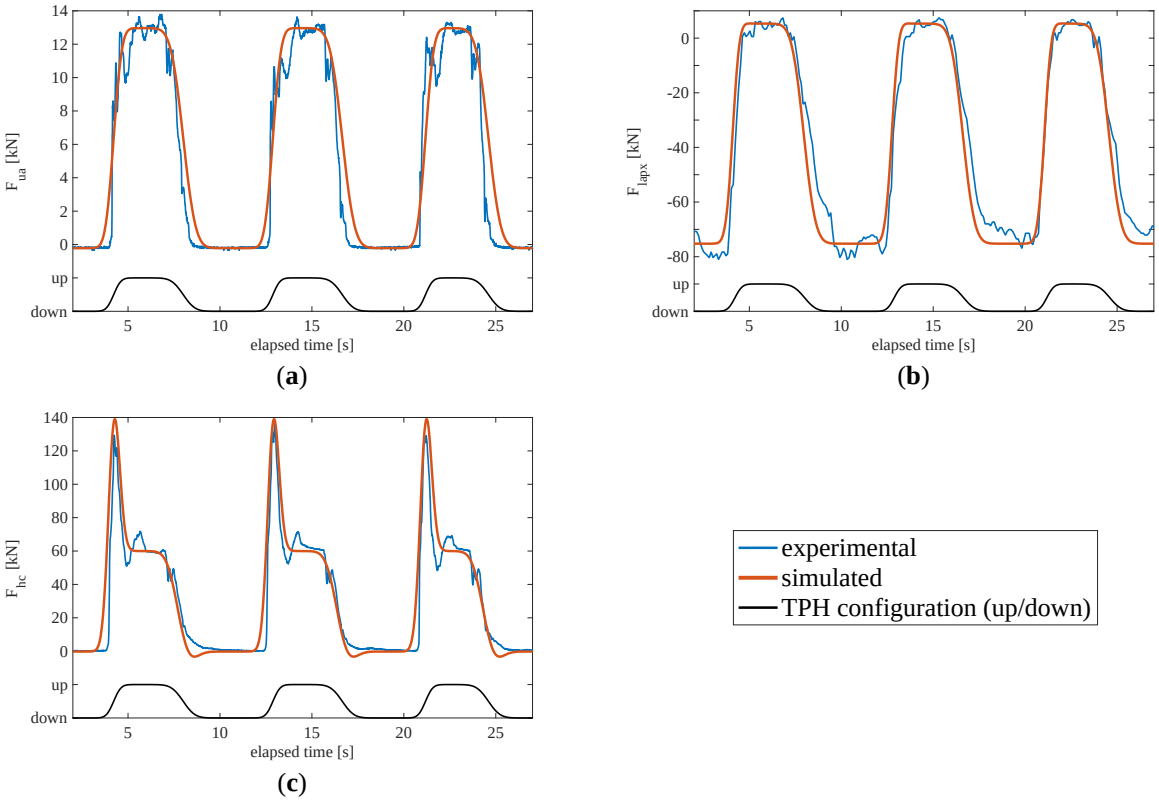

Figure 3.3 Comparison between experimental and simulated force profile during implement maneuvering. (a) Force at the up-per arm; (b) force at the lower link points, horizontal component; (c) force at the hydraulic lift cylinders.

From the field tests, the parameters for the reference maneuver and the reference soil were also determined by taking the values that allowed to best match the experimental measurements (Table 3-2). The subsoiler used in the validation tests was taken as the reference implement for the model.

The predicted loads exchanged between the soil and the implement during the reference maneuver are depicted in Figure 3.5. It can be observed that the horizontal component F_{wx}, Figure 3.5-a, points rearward, exerting a drag force that reaches its maximum when the working depth of the implement is maximum and decreases as the implement is lifted. As it regards the vertical component F_{wy}, Figure 3.5-b, a peak is observed during the reference maneuver which is induced by the behavior of the implement vertical speed (Figure 3.4) and by the fact that the soil-implement loads depend on the speed of extraction of the implement from the soil (Eq. 2.6). The fact that F_{wy} points downward is consistent with the literature

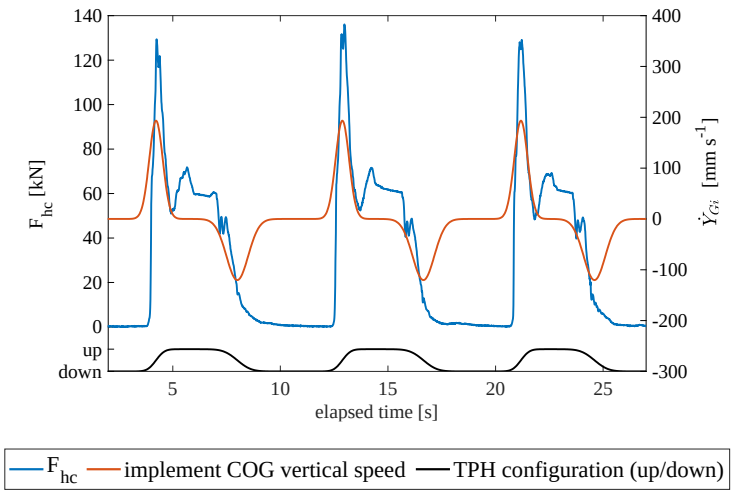

Figure 3.4 Relationship between the force at the hydraulic lift cylinders and the implement COG vertical speed.

(Raper, 2005), and is due to the value of the rake angle of the reference implement shanks, which is smaller than the cross-over value discussed by Godwin (2007) and Godwin and O'Dogherty (2007). Furthermore, the sign of the moment of the resultant about the point P_{lad}, Figure 3.5c, indicates that the line of pull lies below P_{lad} when the implement working depth is maximum, whereas when the working depth is minimum, the horizontal component of the resultant decreases significantly, causing the line of pull to move rearward with respect to P_{lad} and, ultimately, the moment M_w to be negative.

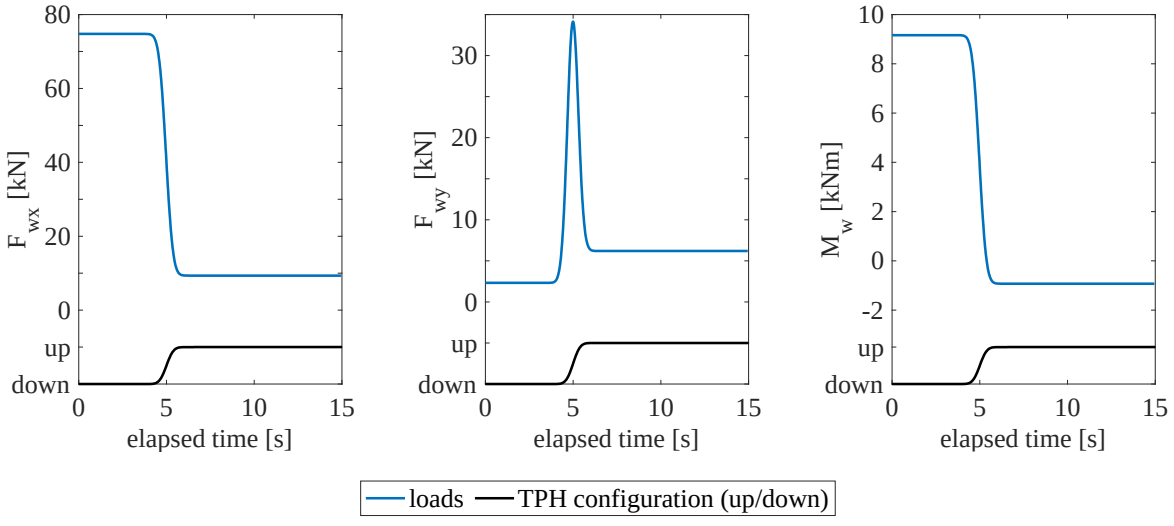

Figure 3.5 Soil-implement system of forces during the reference maneuver: (a) horizontal force (positive if rearward); (b) vertical force (positive if downward); and (c) moment of the resultant about the point P_{lad} (positive if anti-clockwise).

3.2 Simulation of the tractor-TPH-implement aggregate during the reference maneuver

Simulations were performed to show the capabilities of the Optimizer and of the underlying tractor-TPH-implement model. The tractor used for the validation tests was taken as the benchmark for the simulations. As described in Chapter 2, the Optimizer simulates the reference maneuver performed on the reference soil with the reference implement; the values of the maneuver, soil and implement parameters are listed in Table 3-2.

Table 3-2 Parameters used in the simulations.

Reference manoeuvre	T	0.444 s
	t_0	5 s
	$Y_{P_{lad},\min}$	-451 mm (TPH down)
	$Y_{P_{lad},\max}$	-304 mm (TPH up)
Reference implement		Table 3-1
Reference soil	F_{0x}	-125.9 kN
	F_{0y}	14.23 kN
	M_0	$-21.8 \cdot 10^3$ N m
	K_{sx}	0.445 kN mm^{-1}
	K_{sy}	$26.4 \cdot 10^{-3}$ kN mm^{-1}
	K_{sm}	68.6 kN
	C_{sy}^{-}	65 N s mm^{-1}
	C_{sy}^{+}	140 N s mm^{-1}

The values of the tractor parameters used in the simulations are listed in Table 3-3. Spring constants, damping coefficients and tractor moment of inertia were set through the parameter identification procedure described in section 2.6.4 that involved measuring the front axle load during an in-filed maneuver similar to the reference maneuver, performed with the subsoiler used for the validation tests (Table 3-2).

Table 3-3 Tractor parameters used in the tractor dynamic model.

M_t	5975 kg
I_t^{Gz}	5220 kg m^2
M_a	298 kg
l_f	1069 mm
l_r	1491 mm
h_f	195 mm
h_r	20 mm
r_{rw}	877 mm
k_s	$1.10 \cdot 10^5$ N m^{-1}
k_f	$1.00 \cdot 10^6$ N m^{-1}
k_r	$2.10 \cdot 10^6$ N m^{-1}
c_s	$4.60 \cdot 10^3$ N s m^{-1}
c_f	$9.10 \cdot 10^3$ N s m^{-1}
c_r	$1.00 \cdot 10^4$ N s m^{-1}

Figure 3.6 shows a comparative analysis of the behavior of the front axle load during the reference maneuver for the TPH configuration up/down. The loads have been obtained through the simulation of the quasi-static and dynamic tractor models and compared with a front axle load obtained during a real in field maneuver. It can be observed from both simulations how lifting the implement causes the load on the front axle to decrease drastically, this is ultimately due to the peak in the vertical force F_{wy} (Figure 3.5-b). However, at the end of the maneuver, the front axle load obtained with the quasi-static model shows a discrepancy with the one obtained with the dynamic model, the last one exhibits an overshoot, and then a damped oscillation due to the viscoelastic nature of tires and front axle suspension; this behavior is not evidenced in the load obtained with the quasi-static model since the inertial, elastic, and viscous terms are not considered on the model. Accordingly, the proposed quasi-static model does not provide a satisfactory description of the real tractor behavior, while the dynamic model approach shows a more precise result on the vehicle motion by effectively reproducing the lowers and higher peaks existing in the front axle load measured during the experimental in-field maneuver and therefore, allowing to extrapolate

the experimental results over a wide range of test conditions not just for the improvement of the weight transfer effects but also to improve the overall operational performance, comfort, and safety of the tractors. For these reasons, the 3-DOF dynamic tractor model is chosen for the performance evaluation and implementation on the Optimizer.

On the other hand, the reference maneuver proves to be effective in inducing weight transfer from the front to the rear axle and the P2P value of the force on the front axle appears to be a suitable measure of this phenomenon.

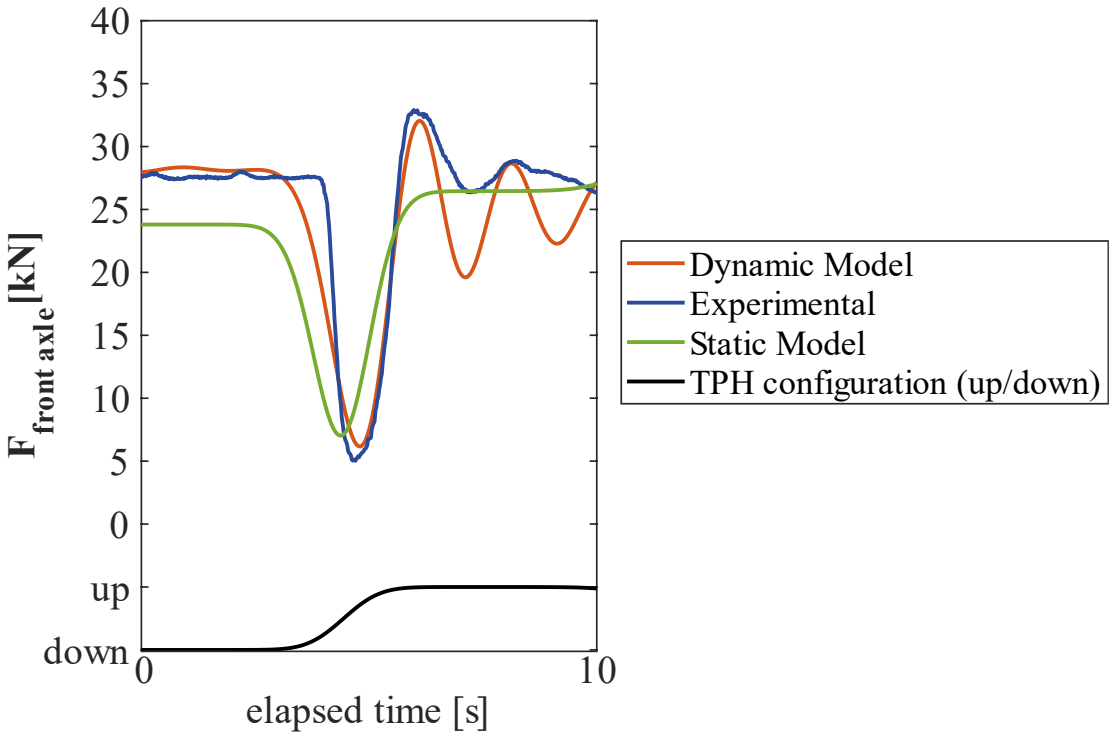

Figure 3.6 Comparative analysis between the experimental front axle load and the simulated front axle load from the quasi-static and the dynamic tractor models.

3.3 Optimization Results and Discussions

To test the capabilities of the Optimizer, a benchmark test was conducted starting from different commercially available category 3 geometries (A, C, G, H). Design considerations led to establish lower and upper bounds on the TPH dimensions subject to optimization (Table 3-4), which were imposed on the Optimizer (Problem 2.27). The dynamic tractor model was used on the calculation of the objective function. The constraints listed in Table-1 were enforced setting the limit values prescribed by the ISO-730 Standard for a category 3 TPH (Table 3-5).

Table 3-4 Lower and upper bounds on the TPH dimensions subject to optimization.

TPH dimension	Lower bound	Upper bound	unit
$X_{P_{cp}}$	140	200	mm
$Y_{P_{cp}}$	325	475	mm
$X_{P_{hcp}}$	235	300	mm
$Y_{P_{hcp}}$	-150	-90	mm
$X_{P_{lap}}$	50	280	mm
$Y_{P_{lap}}$	-270	-180	mm
$X_{P_{uap}}$	275	475	mm
$Y_{P_{uap}}$	200	550	mm
l_c	300	500	mm
l_{chc}	150	350	mm
l_{la}	500	1500	mm
l_{lalr}	250	1000	mm
$l_{lr_{min}}$	400	1200	mm
$l_{lr_{max}}$	400	1200	mm
$l_{ua_{min}}$	400	1200	mm
$l_{ua_{max}}$	400	1200	mm
φ_{chc}	10	45	°
$\varphi_{c_{max}}$	30	80	°
$\varphi_{c_{min}}$	-20	50	°

Table 3-5 ISO-730 functional prescriptions for a category 3 TPH (section 2.6.1 and Table 1).

L_{min}	560 mm
L_{max}	775 mm
L_{14}	230 mm
L_{15}	125 mm
L_{18}	735 mm
L_{19}	106 mm

L_{20}	100 mm
$H_{ma,min}$	230 mm
$H_{ma,max}$	660 mm

Table 3-6 Optimizer performance.

Optimized Config.	**A**	**C**	**G**	**H**	**unit**
$\Phi_{initial}$	25.79	27.07	25.92	26.45	kN
$\Phi_{optimised}$	23.06	23.05	23.01	23.36	kN
reduction in Φ	10.6	**14.9**	11.2	11.7	%
no. of iterations	14	36	26	15	-

Table 3-6 summarizes the performance of the Optimizer starting from the TPH configurations A, C, G, H. Results show that even though starting from different TPH configurations, the tool converges to similar optimized geometries that reduce the P2P at the tractor front axle by around 10% for each configuration. Figure 3.7 shows a comparison between the initial and the optimized TPH geometries A, C, G, H. Additionally, Figure 3.8 shows the initial and optimized front axle load from the four tested configurations A, C, G, H. After 36 iterations, the highest reduction in the P2P of the front axle load value was found on the configuration C, obtaining an optimized geometry with a 14.9% of optimization (Figure 3.7-b and Figure 3.8-b).

Analyzing the optimum configuration C (Figure 3.7-b), it can be observed that the point P_{lap} is shifted towards the rear axle center as much as the bounds on the dimensions $X_{P_{lap}}$ and $Y_{P_{lap}}$ allowed. Furthermore, the point P_{cp} is shifted upward and rearward, while the angle φ_{chc} is considerably smaller than it was in the starting TPH geometry; consequently, the value of the dimension $\varphi_{c_{min}}$ decreased to its lower admissible value. Figure 3.7-b also shows that the point P_{uap} is considerably shifted upward and rearward, the value of the dimension $X_{P_{uap}}$ being equal to its upper admissible value.

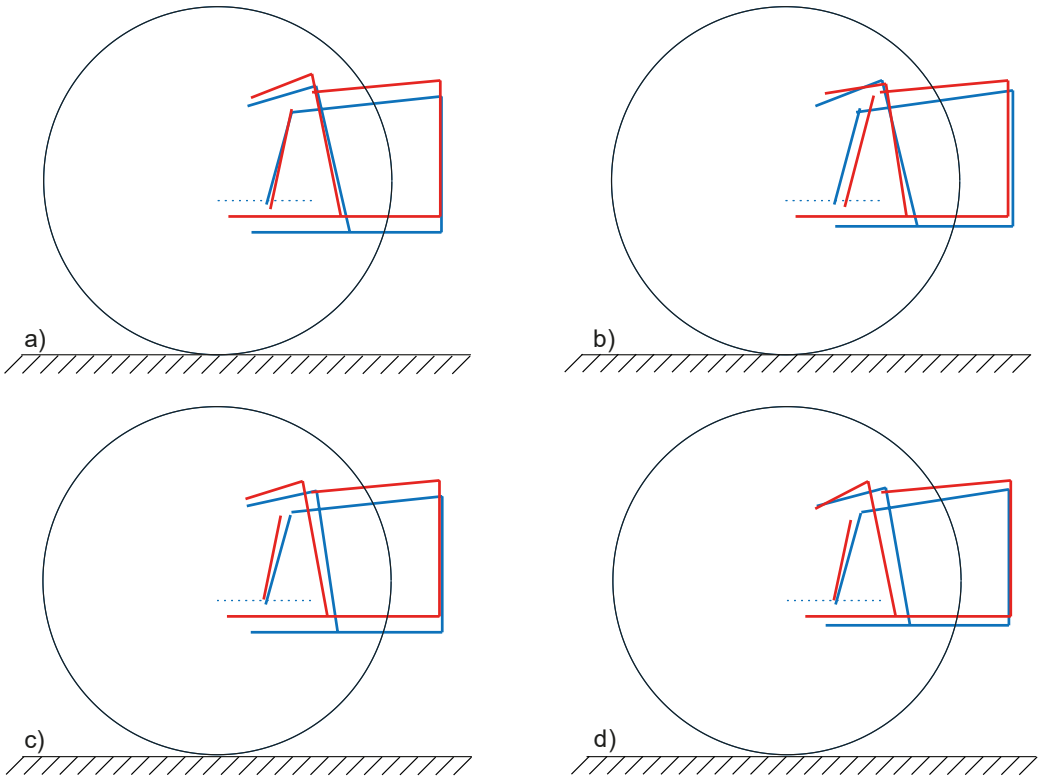

Figure 3-7 Starting Configuration (blue), Optimized Configurations (red). a) Configuration A, b) Configuration C, c) Configuration G, d) Configuration H.

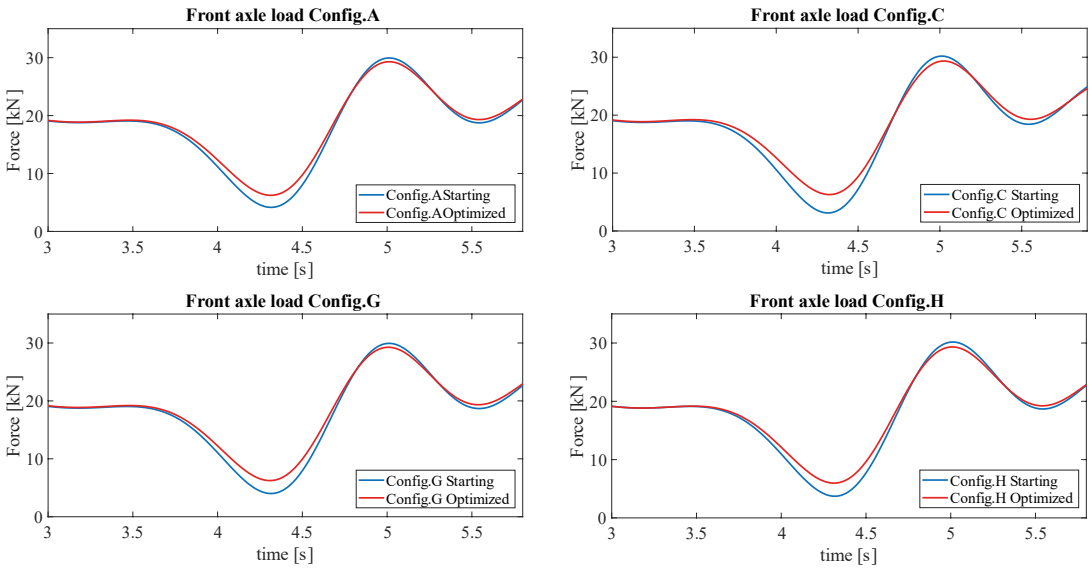

Figure 3-8 Initial and optimized front axle load for the configurations A, C, G, H.

Figure 3.9 shows a comparison between the resulted optimized geometries A, C, G, H. It can be observed that the Optimizer algorithm converges to similar optimized values regarding the following variables: lower link points $X_{P_{lap}}$,$Y_{P_{lap}}$; upper link points $X_{P_{uap}}$, $Y_{P_{uap}}$; lift arm length l_c; upper arm length $l_{ua_{min}}$ and lower arm length L_{la}.

Table 3-7 provides the resulting optimized values regarding the TPH-tested configurations A, C, G, H. Results show that optimized values in the dimension $X_{P_{lap}}$, tend to match the lower bound limit regarding configurations C and G, while, in the case of configurations A and H, the optimum values are slightly displaced from the lower bound value. Regarding the dimension $Y_{P_{lap}}$, the Optimizer converges to the exact value in the four configurations matching the upper bound limit. A similar result is obtained for the variables $X_{P_{uap}}$, $Y_{P_{uap}}$, where the resulted values exactly match the upper bound limit on the dimension $X_{P_{uap}}$ for all the tested configurations, while in the dimension $Y_{P_{uap}}$, the Optimizer converges to almost the exact value for all the configurations. In the case of dimension l_c the Optimizer found relatively close values in the four configurations tending to the lower bound value. However, in the case of the dimension $l_{ua_{min}}$, the optimum values are similar to each other and tend to the upper bound limit value. In the case of the dimension L_{la}, the Optimizer converges to almost the same values for the configuration A, C, and G, while a relatively small value is founded for the configuration H.

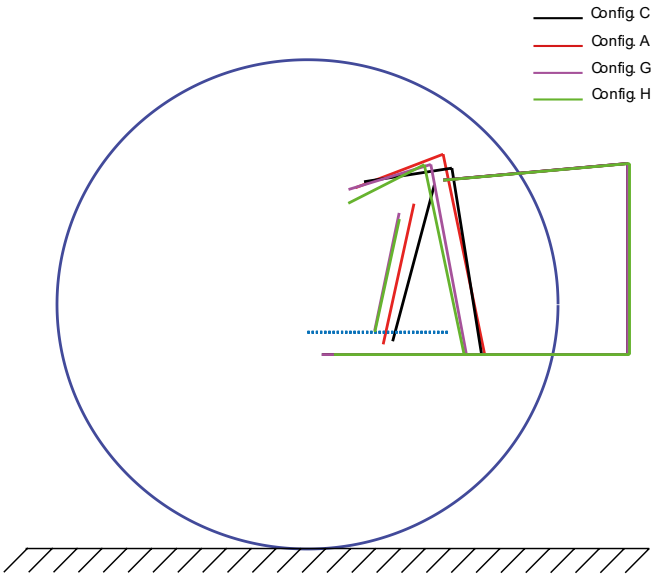

Figure 3-9 Optimized geometries for the configurations A, C, G, H.

Table 3-7 Optimizer results.

TPH dimension	**A_Opt**	**C_Opt**	**G_Opt**	**H_Opt**	**unit**
$X_{P_{cp}}$	167	198	143	143	mm
$Y_{P_{cp}}$	418	440	412	362	mm
$X_{P_{hcp}}$	265	298	235	236	mm
$Y_{P_{hcp}}$	-143	-132	-95	-99	mm
$X_{P_{lap}}$	54	50	50	92	mm
$Y_{P_{lap}}$	-180	-180	-180	-180	mm
$X_{P_{uap}}$	475	475	475	475	mm
$Y_{P_{uap}}$	446	446	446	445	mm
l_c	330	311	302	300	mm
l_{chc}	213	247	196	188	mm
l_{la}	1067	1071	1071	1035	mm
l_{lalr}	567	559	506	456	mm
$l_{lr_{min}}$	800	743	753	750	mm
$l_{lr_{max}}$	666	610	633	639	mm
$l_{ua_{min}}$	927	920	921	925	mm
$l_{ua_{max}}$	556	557	590	622	mm
φ_{chc}	37	12	43	45	°
$\varphi_{c_{max}}$	73	59	66	77	°
$\varphi_{c_{min}}$	-5	-20	-9	3	°

CONCLUSIONS

The current research thesis presents a computational design tool (*The Optimizer*); developed to optimize the geometry of a tractor rear-mounted three-point hitch (TPH) in order to minimize the weight transfer from the front to the rear tractor axle during implement operation or maneuvering. To this end, the Optimizer simulates a reference maneuver performed with a reference implement on a reference soil. Simulations are based on a dynamic model of the tractor-TPH-implement aggregate. The following conclusions can be drawn from the study:

- A constrained minimization algorithm was defined for the optimization of a tractor TPH geometry. The algorithm evaluates a trial TPH geometry pertaining to a predefined category searching to minimize at each step of iteration the front-to-rear axle load transfer, defined as the objective function of the optimization problem. Constraints arise from the ISO-730 standard and other design constraints set to guarantee the algorithm's correctness in functionality and robustness. A TPH geometry that minimizes the objective function and respects all the constraints is found as result of the iteration process.

- The proposed reference maneuver was defined in a general manner based on the ISO-730 functional requirements such that, all the TPH existing categories can accurately reproduce real infield implement maneuvering. Furthermore, simulation results suggest that the defined reference maneuver is effective in triggering the weight-transfer effect.

- The soil-implement interaction model developed in this study has been defined by assuming the exchange of forces between the soil and the implement to vary only as function of the implement working depth and the speed of penetration/extraction of the implement into/from the soil, while the remaining parameters are defined as constants. The model was implemented in the Optimizer and successfully validated against infield test data, enabling a more accurate assessment of the load transfer effects.

- The evaluation of the front-to-rear axle load transfer is carried out through the simulation of the dynamic tractor-TPH-implement aggregate model. The peak-to-peak (P2P) value of the front axle load during the reference maneuver is adopted as the measure of the weight transfer, thus, has been defined as the objective function. Simulation findings indicate that the P2P seems to be a good measure of the study phenomenon.

- For the development of the tractor model, two alternatives were studied: a quasi-static model and a 3-DOF dynamic model. The resulting front axle load obtained with the quasi-static tractor model and the one obtained with the dynamic tractor model were compared with a real front axle load measured during an experimental in-field maneuver. The inertial, elastic, and viscous parameters of the dynamic model were successfully determined through a parameter identification algorithm. The comparative investigation revealed that the quasi-static model failed to accurately describe the real tractor behavior to replicate the weight transfer effect. On the other hand, the dynamic model approach provides a more precise result able to reproduce the lower and higher peaks present on the front axle load measured during the experimental in-field maneuver and caused by the weight transfer, thus, allowing to extrapolate the experimental results over a wide range of test conditions for the overall improvement of operational performance, comfort, and safety of agricultural tractors. For that reason, the 3DOF dynamic tractor model was chosen to be implemented on the Optimizer algorithm.

- The Optimizer was subjected to a benchmark test starting from four geometries of a commercially available TPH. The test showed that even though starting from different initial configurations, the algorithm converges to similar optimized geometries, reducing the weight transfer effect by above 10% and reaching a maximum optimization of 14.9 % in one of the tested configurations, thus demonstrating the robustness of the algorithm.

- Simulation results prove that the Optimizer is an effective and efficient design tool able to simplify the exploration of the design parameters conforming a TPH geometry, thus, demonstrating that the Optimizer can be applied in practical applications, improving the efficiency of the engineering design process and consequently the operational performance, comfort, and safety of agricultural tractors.

REFERENCES

Ahmadi, I. (2011). Dynamics of tractor lateral overturn on slopes under the influence of position disturbances (model development). *Journal of Terramechanics, 48*(5), 339-346. https://doi.org/10.1016/J.JTERRA.2011.07.001

Ambike, S. S., & Schmiedeler, J. P. (2007). Application of Geometric Constraint Programming To The Kinematic Design of Three-Point Hitches. *Applied Engineering in Agriculture, 23*(1), 13-21. https://doi.org/10.13031/2013.22325

ASAE Standards. (2001). *S217.12: Three-point free-link attachment for hitching implements to agricultural wheel tractors*.

Avello Fernández, L., Maraldi, M., Mattetti, M., & Varani, M. (2022). *A Computational Tool for Three-Point Hitch Geometry Optimisation Based on Weight-Transfer Minimisation*. https://doi.org/10.3390/agriculture12040460

Baillie, C. P., Lobsey, C. R., Antille, D. L., McCarthy, C. L., & Thomasson, J. A. (2018). *A review of the state of the art in agricultural automation. Part III: Agricultural machinery navigation systems*. 1.

Baillie, C. P., Thomasson, J. A., Lobsey, C. R., McCarthy, C. L., & Antille, D. L. (2018). *A review of the state of the art in agricultural automation. Part I: Sensing technologies for optimization of machine operation and farm inputs*. 1.

Bauer, F., Porteš, P., Slimařík, D., Čupera, J., & Fajman, M. (2017). Observation of load transfer from fully mounted plough to tractor wheels by analysis of three point hitch forces during ploughing. *Soil and Tillage Research, 172*, 69-78.

Collins, T. S. (1991). Loads in tractor linkages when transporting rear-mounted implements: Development of modelling and measurement techniques. *Journal of Agricultural Engineering Research, 49*(C), 165-188. https://doi.org/10.1016/0021-8634(91)80037-F

Dhruw, L. K., Pareek, C. M., & Singh, N. (2018). A Visual Basic Programme for Performance Evaluation of Three-point Linkage Hitch System of Agricultural Tractors. *Current Journal of Applied Science and Technology*.

Gobbi, M., Mastinu, G., & Previati, G. (2014). Farm tractors with suspended front axle: Anti-dive and anti-lift characteristics. *Journal of Terramechanics*, *56*, 157-172. https://doi.org/10.1016/J.JTERRA.2014.10.003

Godwin, R. J. (2007). A review of the effect of implement geometry on soil failure and implement forces. *Soil and Tillage Research*, *97*(2), 331-340. https://doi.org/10.1016/J.STILL.2006.06.010

Godwin, R. J., & O'Dogherty, M. J. (2007). Integrated soil tillage force prediction models. *Journal of Terramechanics*, *44*(1), 3-14. https://doi.org/10.1016/j.jterra.2006.01.001

Godwin, R. J., O'Dogherty, M. J., Saunders, C., & Balafoutis, A. T. (2007). A force prediction model for mouldboard ploughs incorporating the effects of soil characteristic properties, plough geometric factors and ploughing speed. *Biosystems Engineering*, *97*(1), 117-129. https://doi.org/10.1016/J.BIOSYSTEMSENG.2007.02.001

Godwin, R. J., & Spoor, G. (1977). Soil failure with narrow tines. *Journal of Agricultural Engineering Research*, *22*(3), 213-228. https://doi.org/10.1016/0021-8634(77)90044-0

Godwin, R. J., & Wheeler, P. N. (1996). An investigation into the soil mechanics of land anchors. *Journal of agricultural engineering research*, *63*(1), 53-59.

Grečenko, A. (1968). Predicting the performance of wheel tractors in combination with implements. *Journal of Agricultural Engineering Research*, *13*(1), 49-63. https://doi.org/10.1016/0021-8634(68)90120-0

Guzzomi, A. L. (2012). A revised kineto-static model for Phase I tractor rollover. *Biosystems Engineering*, *113*(1), 65-75. https://doi.org/10.1016/J.BIOSYSTEMSENG.2012.06.007

Hettiaratchi, D. R. P., & Reece, A. R. (1974). The Calculation of Passive Soil Resistance. *Geotechnique*, *24*(3), 289-310. https://doi.org/10.1680/geot.1974.24.3.289

Ibrahmi, A., Bentaher, H., Hamza, E., Maalej, A., & Mouazen, A. M. (2015). Study the effect of tool geometry and operational conditions on mouldboard plough forces and energy requirement: Part 2. Experimental validation with soil bin test. *Computers and Electronics in Agriculture*, *117*, 268-275. https://doi.org/10.1016/J.COMPAG.2015.08.004

Ibrahmi, A., Bentaher, H., Hbaieb, M., Maalej, A., & Mouazen, A. M. (2015). Study the effect of tool geometry and operational conditions on mouldboard plough forces and

energy requirement: Part 1. Finite element simulation. *Computers and Electronics in Agriculture*, *117*, 258-267. https://doi.org/10.1016/J.COMPAG.2015.08.006

ISO. (2009). *ISO - ISO 730:2009—Agricultural wheeled tractors—Rear-mounted three-point linkage—Categories 1N, 1, 2N, 2, 3N, 3, 4N and 4*.

Jazar, R. N. (2017). *Vehicle dynamics: Theory and application*. Springer.

Johansson, S. (2008). Design of a three-point hitch. En *Linköpking University*.

Kabir, M. S. N., Ryu, M.-J., Chung, S.-O., Kim, Y.-J., Choi, C.-H., Hong, S.-J., & Sung, J.-H. (2014). Research trends for performance, safety, and comfort evaluation of agricultural tractors: A review. *Journal of Biosystems engineering*, *39*(1), 21-33.

Kim, K. U., & Rehkugler, G. E. (1987). A Review of Tractor Dynamics and Stability. *Transactions of the American Society of Agricultural Engineers*, *30*(3), 615-623. https://doi.org/10.13031/2013.30449

Kumar, A., Pranav, P. K., & Kumar, S. (2018). Computer simulation of three-point linkage parameters for virtual hitch point and optimum depth of operation. *Engineering in Agriculture, Environment and Food*, *11*(3), 114-121. https://doi.org/10.1016/J.EAEF.2018.02.006

Li, Z., Mitsuoka, M., Inoue, E., Okayasu, T., & Hirai, Y. (2015). Development of stability indicators for dynamic Phase I overturn of conventional farm tractors with front axle pivot. *Biosystems Engineering*, *134*, 55-67. https://doi.org/10.1016/j.biosystemseng.2015.03.016

Macmillan, R. H. (2003). The mechanics of tractor-implement performance. *Agricultural Engineering International: CIGR Journal*.

Mattetti, M., Molari, G., & Sereni, E. (2017). Damage evaluation of driving events for agricultural tractors. *Computers and Electronics in Agriculture*, *135*, 328-337.

McKyes, E. (1985). *Soil cutting and tillage*. Elsevier.

Melzi, S., Negrini, S., & Sabbioni, E. (2014). Numerical analysis of the effect of tire characteristics, soil response and suspensions tuning on the comfort of an agricultural vehicle. *Journal of Terramechanics*, *55*, 17-27. https://doi.org/10.1016/j.jterra.2014.05.001

Molari, G., Mattetti, M., & Guarnieri, A. (2014). Optimal three-point hitch design to maximize lifting performance. *Transactions of the ASABE*, *57*(2), 371-379.

Morling, R. W. (1979). AGRICULTURAL TRACTOR HITCHES - ANALYSIS OF DESIGN REQUIREMENTS. *ASAE Distinguished Lecture Series: Tractor Design*, *5*, 5-.

Oberhaus, C., Biller, R. H., Brunswick, G., Keuper, P., & Stachnik, P. (2005). Load transfer from the fully-mounted plough on the tractor. *Landtechnik, 6*, 330-331.

OECD. (2012). *CODE 2-OECD standard code for the official testing of agricultural and forestry tractor performance*. Organization for Economic Cooperation and Development (OECD): Paris, France.

Payne, P. C. J. (1956). The relationship between the mechanical properties of soil and the performance of simple cultivation implements. *Journal of Agricultural Engineering Research, 1*(1), 23-50.

Payne, P. C. J., & Tanner, D. W. (1959). The relationship between rake angle and the performance of simple cultivation implements. *Journal of Agricultural Engineering Research, 4*(4), 312-325.

Pearson, P., & Bevly, D. M. (2007). Modeling and validation of hitch loading effects on tractor yaw dynamics. *Journal of Terramechanics*, *44*(6), 439-450. https://doi.org/10.1016/J.JTERRA.2008.03.001

Porteš, P., Bauer, F., & Čupera, J. (2013). Laboratory-experimental verification of calculation of force effects in tractor's three-point hitch acting on driving wheels. *Soil and Tillage Research, 128*, 81-90. https://doi.org/10.1016/j.still.2012.10.007

Prasanna Kumar, G. V. (2012). Development of a computer program for the path generation of tractor hitch points. *Biosystems Engineering*, *113*(3), 272-283. https://doi.org/10.1016/J.BIOSYSTEMSENG.2012.09.004

Previati, G., Gobbi, M., & Mastinu, G. (2007). Farm tractor models for research and development purposes. *Vehicle System Dynamics*, *45*(1), 37-60. https://doi.org/10.1080/00423110600833400

Previati, G., Gobbi, M., & Mastinu, G. (2011). Multi-objective-reliability-based optimisation of a farm tractor front axle suspension. *International Journal of Heavy Vehicle Systems, 18*(3), 257-271. https://doi.org/10.1504/IJHVS.2011.041590

Qin, J., Zhu, Z., Ji, H., Zhu, Z., Li, Z., Du, Y., Song, Z., & Mao, E. (2019). Simulation of active steering control for the prevention of tractor dynamic rollover on random road surfaces. *Biosystems Engineering*, *185*, 135-149. https://doi.org/10.1016/J.BIOSYSTEMSENG.2019.02.006

Rabbani, M. A., Tsujimoto, T., Mitsuoka, M., Inoue, E., & Okayasu, T. (2011). Prediction of the vibration characteristics of half-track tractor considering a three-dimensional dynamic model. *Biosystems Engineering*, *110*(2), 178-188. https://doi.org/10.1016/J.BIOSYSTEMSENG.2011.07.013

Raper, R. (2005). FORCE REQUIREMENTS AND SOIL DISRUPTION OF STRAIGHT AND BENTLEG SUBSOILERS FOR CONSERVATION TILLAGE SYSTEMS. *Applied Engineering in Agriculture*, *21*(5), 787-794.

Saunders, C., Godwin, R. J., & O'Dogherty, M. J. (2000). Prediction of soil forces acting on mouldboard ploughs. *Fourth International Conference on Soil Dynamics, Adelaide*.

Shmulevich, I. (2010). State of the art modeling of soil–tillage interaction using discrete element method. *Soil and Tillage Research*, *111*(1), 41-53. https://doi.org/10.1016/J.STILL.2010.08.003

Srivastava, A. K., Goering, C. E., Rohrbach, R. P., & Buckmaster, D. R. (2006). *Engineering Principles of Agricultural Machines*.

Sunusi, I. I., Zhou, J., Wang, Z. Z., Sun, C., Ibrahim, I. E., Opiyo, S., Soomro, S. A., Sale, N. A., & Olanrewaju, T. (2020). Intelligent tractors: Review of online traction control process. *Computers and electronics in agriculture*, *170*, 105176.

Thomasson, J. A., Baillie, C. P., Antille, D. L., McCarthy, C. L., & Lobsey, C. R. (2018). *A review of the state of the art in agricultural automation. Part II: On-farm agricultural communications and connectivity*. 1.

Zheng, E., Cui, S., Yang, Y., Xue, J., Zhu, Y., & Lin, X. (2019). Simulation of the vibration characteristics for agricultural wheeled tractor with implement and front axle hydropneumatic suspension. *Shock and Vibration*, *2019*.

Zheng, E., Zhong, X., Zhu, R., Xue, J., Cui, S., Gao, H., & Lin, X. (2019). Investigation into the vibration characteristics of agricultural wheeled tractor-implement system with hydro-pneumatic suspension on the front axle. *Biosystems Engineering*, *186*, 14-33.